Nano-Micro Letters
e-ISSN 2150-5551
CN 31-2103/TB
REVIEW
https://doi.org/10.1007/s40820-022-00944-z

Cite as
Nano-Micro Lett.
(2022) 14:199

Received: 28 June 2022
Accepted: 31 August 2022

Animal- and Human-Inspired Nanostructures as Supercapacitor Electrode Materials: A Review

Iftikhar Hussain[1], Charmaine Lamiel[2], Sumanta Sahoo[3], Muhammad Sufyan Javed[4], Muhammad Ahmad[1], Xi Chen[1], Shuai Gu[1], Ning Qin[1], Mohammed A. Assiri[5], Kaili Zhang[1] ✉

HIGHLIGHTS

- Animal- and human-inspired nanostructures as supercapacitor electrode materials are summarized.
- Structural formation and supercapacitive electrochemical applications are comprehensively summarized.
- Future outlooks such as large-scale production and other properties are proposed.

ABSTRACT Human civilization has been relentlessly inspired by the nurturing lessons; nature is teaching us. From birds to airplanes and bullet trains, nature gave us a lot of perspective in aiding the progress and development of countless industries, inventions, transportation, and many more. Not only that nature inspired us in such technological advances but also, nature stimulated the advancement of micro- and nanostructures. Nature-inspired nanoarchitectures have been considered a favorable structure in electrode materials for a wide range of applications. It offers various positive attributes, especially in energy storage applications, such as the formation of hierarchical two-dimensional and three-dimensional interconnected networked structures that benefit the electrodes in terms of high surface area, high porosity and rich surface textural features, and eventually, delivering high capacity and outstanding overall material stability. In this review, we comprehensively assessed and compiled the recent advances in various nature-inspired based on animal- and human-inspired nanostructures used for supercapacitors. This comprehensive review will help researchers to accommodate nature-inspired nanostructures in industrializing energy storage and many other applications.

KEYWORDS Nature-inspired nanostructure; Supercapacitors; Energy storage; Animal-inspired and human-inspired nanostructures

Iftikhar Hussain, Charmaine Lamiel, and Sumanta Sahoo have contributed equally to this work.

✉ Kaili Zhang, kaizhang@cityu.edu.hk
[1] Department of Mechanical Engineering, City University of Hong Kong, 83 Tat Chee Avenue, Kowloon, Hong Kong, People's Republic of China
[2] Department of Chemical Engineering, University of Wyoming, Laramie, WY 82071, USA
[3] Department of Chemistry, Madanapalle Institute of Technology and Science, Madanapalle, Andhra Pradesh 517325, India
[4] School of Physical Science and Technology, Lanzhou University, Lanzhou 730000, People's Republic of China
[5] Department of Chemistry, Faculty of Science, King Khalid University, Abha 61413, Saudi Arabia

Published online: 06 October 2022

1 Introduction

Over the years, nature plays an important role in the development of mankind. Many revolutionary discoveries of today's world have been inspired by nature. In the area of materials science, such inspiration from nature has been successively employed in fabrication processes as well as to design target materials. The highly ordered, diverse, and unique structures of natural things and biomaterials inspired researchers to duplicate and mimic it in nanomaterials through material chemistry [1–7]. The inspiration from nature and the designing of nanomaterials with appropriate orientation, highly ordered structure, and exceptional mechanical robustness while achieving high energy and power densities have remained a hot topic in developing electrode materials. Many nature-inspired commercial products are also easily available in today's commercial market [8]. For example, artificial photosynthesis, inspired by the photosynthesis of plant, approach has been successively employed for harvesting solar energy [9, 10]. Other nature-inspired applications include bio-inspired water purification system [11], protein production inspired from the silk making process of spiders [12], bio-inspired materials for plastic replacement [13], etc. have also been reported. Moreover, nature-inspired materials and designs have also been explored to produce natural and renewable resources toward sustainable, low-cost electrode development [14– 17].

The enthusiastic development of cutting-edge energy storage devices advances today's electronics world for the betterment of tomorrow. Supercapacitors (SCs) are one of such elite electrochemical energy storage devices which have gained enormous research interest in last few years [18–27]. Specially, the charge storage mechanism of electric double layer capacitor (EDLC) does not involve any chemical reaction [28– 30], which plays a crucial role for the designing of sustainable future. Benefitted by their enhanced charge storage mechanism, improved cycling stability, high rate capability, and elevated power density, SCs have shown promising advantages to fulfill the demand of future electronic devices [31– 38]. In this aspect, several strategies have been employed for enhancing the capacitive performance of SC electrodes. Among them, high porosity, high conductivity, and large surface area are some of the prime factors being considered [39– 42]. Basically, the porous nature of electrode materials allows easy and fast transport of electrolyte ions which further improves the electrochemical performance [43– 49]. While these properties are important, the morphology of the electrode materials is equally significant too [50–55]. The availability of large electrochemical surface area also relieves the stress incurred by long charging/discharging cycles. Among different morphologies, hierarchical morphologies are advantageous toward energy storage application due to their enhanced surface area, low density, controlled, interconnected structure, and enhanced accessible area. Such materials produce electrical, chemical, biological, mechanical, as well as sustainable gains, which are valuable toward the new developments in the energy-related fields [8]. In this aspect, nature-inspired materials with hierarchical structures are highly beneficial, such as, carbon materials with nature-inspired structures displaying high surface area and enhanced porosity. On the other hand, some metal oxides/mixed metal oxides also exhibited promising electrochemical characteristics, benefitted by their special nanoarchitectures [56– 59]. Although the nature-inspired materials are long way to go for commercialization, the current research trend is very encouraging for sustainable future. Despite of their impressive characteristics, very few systematic review articles on energy-related applications of nature-inspired materials are available [1, 6, 7, 60, 61]. Therefore, a timely update on such materials in this particular research field is highly necessary.

The aim of this paper is to summarize the applications of nature-inspired (animal- and human body-inspired) morphologies comprehensively for SC as shown in Fig. 1. Categorizing nature-inspired nanostructures according to a group of animal-inspired (honeycomb-, beehive-, spider web-, hedgehog-, whisker-, caterpillar and worm-, nest-, and plume-like) and human body-inspired (spine-, finger-, DNA-, and dendrite-like) nanostructures. This review discusses different factors and certain conditions capable of generating nature-inspired nanostructures. Moreover, the review ends with incorporating the learning from nature-inspired nanostructures with outlook, prospects, and strategies to mitigate the shortcomings of future electrodes in SC and battery applications.

https://doi.org/10.1007/s40820-022-00944-z

Fig. 1 Schematic illustration of animal- and human body-inspired nanostructures

2 Nature-Inspired Structures: Synthesis, Structural Formation, and Supercapacitive Electrochemical System Application

As categorized in the dimensional growth of structures, the formation of 0D, 1D, 2D, and 3D structures are widely investigated in the mechanistic formation of crystals and their morphology [62–66]. Tiwari et al. [67] categorized different nanostructured materials as 0D, such as uniform particles arrays (quantum dots), heterogeneous particles arrays, core–shell quantum dots, onions, hollow spheres, and nanolenses; 1D such as nanowires, nanorods, nanotubes, nanobelts, and nanoribbons; 2D such as junctions (continuous islands), branched structures, nanoprisms, nanoplates, nanosheets, nanowalls, and nanodisks; and 3D such as nanoballs (dendritic structures), nanocoils, nanocones, nanopillars, and nanoflowers.

Even though these structures are classified into dimensional orientations, many studies have shown nanostructures mimicking things that we regularly see in nature. The overlapping and combination of 1D, 2D, and 3D nanostructures that resemble trees, honeycombs, flowers, urchins, etc., have been synthesized and worked effectively as an electrode material for SCs. Depending on many factors, such as choice of precursors, method of synthesis, the structure of an active electrode material can be customized in a way that more surface area can be exposed [53– 55, [68]. For example, carbon with tailored structure can achieve high surface area by engineering its morphology [69– 72] (Table 1). Such engineering of structures paved way for researchers to continuously study and evaluate hierarchical structures in a nanoscale level [73– 75].

In this section, we discuss the recent morphologies reported that imitate various nature-inspired such as animal and human body-inspired nanostructures, their method of synthesis, and their electrochemical properties applied as SC. This section is divided into groups according to animal-inspired (honeycomb-, beehive-, spider web-, hedgehog-, whisker-, caterpillar and worm-, nest-, and plume-like) and human body-inspired (spine-, finger-, DNA-, and dendrite-like) nanostructures.

Table 1 Specific surface area of carbon with various animal- and human-inspired structures

Nature-inspired structure	Electrode material	Specific surface area (m^2 g^{-1})	Refs.
Beehive-like	Porous carbon	1472	[76]
Beehive-like	Microporous carbon	1327	[77]
Beehive-like	Porous carbon	1615	[78]
Honeycomb-like	Graphene	1962	[79]
Honeycomb-like	activated carbon	2990	[80]
Whisker-like	N-doped hollow porous carbons	3007	[81]
Worm-like	Nitrogen, sulfur-co-doped hierarchical porous carbon	720	[82]
Nest-like	N- and P-co-doped mesoporous carbon	922	[83]
Spine-like	Nanostructured carbon interconnected by graphene	428	[84]

2.1 Animal-Inspired Structures

2.1.1 Honeycomb-Like Structure

With a similar structure, honeycomb and beehive-like structures have uniform and regularly shaped pores. Bio-inspired honeycomb-like [85–92] and beehive-like [76, 93, 94] structures with vertical thin walls have been greatly studied for SCs due to its excellent mechanical properties as well as exceptional active sites [2, 92, [95– 99]. Aside from SCs, bio-inspired honeycomb structures have also inspired further applications in biomedicine such as tissue engineering and regenerative medicine [97].

Lv et al. [100] reported novel honeycomb-lantern-inspired 3D flexible and stretchable SCs for improved capacitance. The interesting structural flexibility and stretchability in shape of honeycomb-like structure offer mechanical strength as shown in Fig. 2a. The honeycomb-lantern-inspired structure was synthesized based on expandable composite electrode composed of polypyrrole/black-phosphorous oxide electrodeposited on carbon nanotube (CNT) film. The 3D honeycomb-lantern-inspired exhibited enhanced stretchability compared to 2D counterparts, which is useful for wearable devices. More importantly, the device is feasible to lessen the stress from different directions. The 3D SC maintained a capacitance of 95% under the reversible strain of 2000% even after 10,000 stretch and release cycles. Sun et al. [101] reported the metal–organic frameworks (MOFs) as a sacrificial template to prepared honeycomb-like metal sulfide as a SC electrode. Among different electrode materials, the MOF-derived honeycomb-like metal sulfide at 500 °C (Co_9S_8@C-500) exhibited superior performance due to enhanced active sites of porous carbon thin nanosheets (Fig. 2b), which suppressed the agglomeration of metal sulfide and the improved conductivity of the electrode material due to carbon nanosheets. The Co_9S_8@C-500 exhibited no fade in capacitance for 4000 cycles, confirming its excellent mechanical properties. Peng et al. [102] compared dynamic hydrolysis and static deposition approaches for the fabrication of SC electrode materials. Ruthenium oxide hollow sphere (static deposition) and honeycomb-like (dynamic hydrolysis) nanostructure were compared. The ruthenium oxide honeycomb-like (RHCs) electrode exhibited superior surface area (226 m^2 g^{-1}) than ruthenium oxide hollow sphere (RHSs)-like (226 m^2 g^{-1}) structure (Fig. 2c-d). Furthermore, the honeycomb-like electrode exhibited 5% higher cycling stability for the same number of cycles. Wu et al. [99] carbonized KOH-treated wheat flour in a single

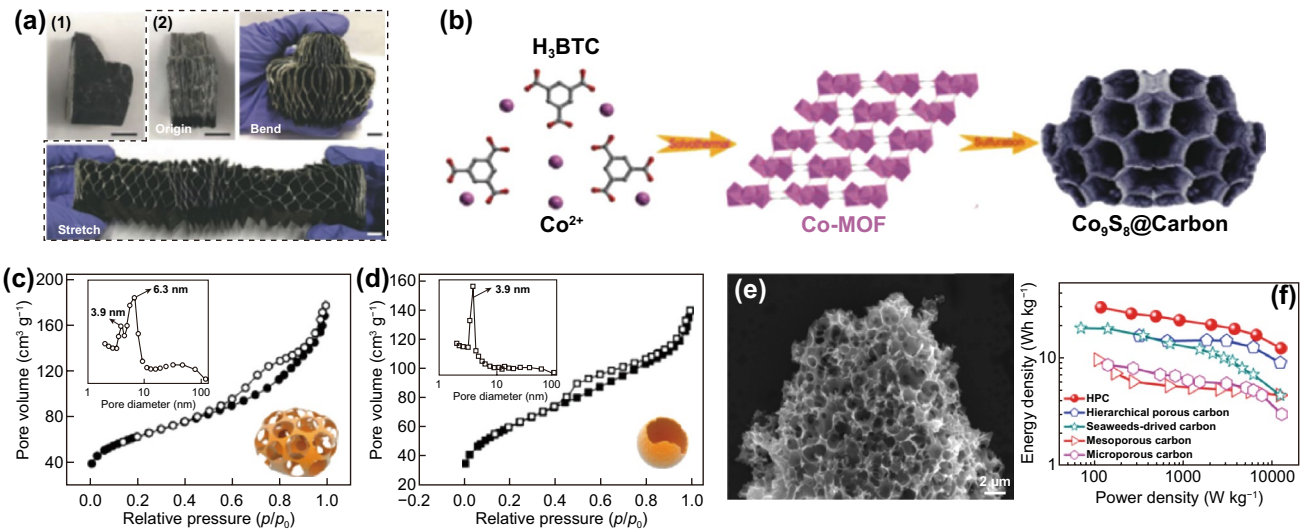

Fig. 2 **a** 3D stretchable supercapacitors with various shape. Reproduced with permission from Ref. [100]. Copyright 2018, Wiley–VCH; **b** Schematic illustration of Co_9S_8@C-500 synthesis strategy. Reproduced with permission from Ref. [101]. Copyright 2018, Wiley–VCH; N_2 adsorption (close symbol)–desorption (open symbol) isotherms of $RuO_2{\cdot}xH_2O$ 3D architectures **c** RHCs and **d** RHSs; inset shows the corresponding BJH pore size distribution curves obtained from the desorption branch. Reproduced with permission from Ref. [102]. Copyright 2017, ACS Publications; **e** SEM image of HPC, **f** Ragone plots of the HPC symmetrical supercapacitor Reproduced with permission from Ref. [99]. Copyright 2015, Elsevier

 https://doi.org/10.1007/s40820-022-00944-z

Table 2 Comparison of animal-inspired structures in three-electrode measurements

Electrode structure	Electrode materials	Method	Three-electrode measurements			Refs.
			Capacitance	Cycling Stability	Electrolyte	
Animal-inspired structures						
Honeycomb and beehive-like structures						
Honeycomb	N-doped porous carbon	Carbonization	275 F g^{-1} 0.5 A g^{-1}	99% 5,000 cycles 1 A g^{-1}	6 M KOH	[143]
Honeycomb	$FeMoO_4$ on NF	CBD	158.39 mA h g^{-1} 2 A g^{-1}	90.76% 4,000 cycles 6 A g^{-1}	3 M KOH	[92]
Honeycomb	Porous carbon	Carbonization	349 F g^{-1} 1 A g^{-1}	98.6% 10,000 cycles 200 mV s^{-1}	6 M KOH	[144]
Honeycomb	NiO	Hydrothermal	1,250 F g^{-1} 1 A g^{-1}	88.4% 3,500 cycles 5 A g^{-1}	6 M KOH	[145]
Honeycomb	Porous carbon	Hydrothermal, carbonization	227 F g^{-1} 1.5 mA cm^{-2}	100% 2,000 cycles 40 mA cm^{-2}	2 M KOH	[146]
honeycomb	$NiCo_2O_4$ on NF	Combustion method	646.6 F g^{-1} 1 A g^{-1}	NA	6 M KOH	[98]
Honeycomb	O, N- carbon	Ethanol extraction, chemical activation	381 F g^{-1} 1 A g^{-1}	NA	6 M KOH	[147]
			160 F g–1 1 A g–1	NA	1 M KOH	
honeycomb	Mo-ZnS@NF	hydrothermal	2,208 F g^{-1} 1 A g^{-1}	83.5% 5,000 cycles 10 A g^{-1}	3 M KOH	[148]
Honeycomb	rGO/NiO/Co_3O_4	Microwave irradiation	910 F g^{-1} 20 mV s^{-1}	89.9% 2,000 cycles 100 mV s^{-1}	0.1 M KOH	[149]
Honeycomb	rGO/Co_2SiO_4	Hydrothermal	429 F g^{-1} 0.5 A g^{-1}	92% 10,000 cycles NA	3 M KOH	[150]
Honeycomb	$Ni_{0.85}Se$ on NF	Hydrothermal	3,105 F g^{-1} 1 A g^{-1}	90.1% 5,000 cycles 10 A g^{-1}	3 M KOH	[151]
Other animal-inspired structures						
Beehive	porous carbon	Carbonization, activation	314 F g^{-1} 0.5 A g^{-1}	96% 2,000 cycles 5 A g^{-1}	6 M KOH	[94]
Beehive	$NiFe_2O_4$/ Ni nanocone on Ni foil	Electrodeposition	483 F g^{-1} 5 A g^{-1}	95.3% 10,000 cycles NA	1 M KOH	[93]
web	V_3O_7 on carbon cloth	Hydrothermal	198 F g^{-1} 1 A g^{-1}	~97% 100,000 cycles 10 A g^{-1}	1 M Na_2SO_4	[118]
Hedgehog	Ni–Mn oxide	Hydrothermal	1,016 F g^{-1} 0.5 A g^{-1}	NA	6 m KOH	[121]
	Ni–Mn sulfide		1,430 F g^{-1} 0.5 A g^{-1}	NA		
Hedgehog	$NiCo_2O_4$ @$Ni_xCo_yMoO_4$	Two-step hydrothermal	861.3 C g^{-1} 1 A g^{-1}	99.5% 10,000 cycles 5 A g^{-1}	PVA-KOH	[119]

Table 2 (continued)

Electrode structure	Electrode materials	Method	Three-electrode measurements			Refs.
			Capacitance	Cycling Stability	Electrolyte	
Whisker	PANI on carbon fibers	Chemical polymerization	427 F g^{-1} 5 mV s^{-1}	90% 3,000 cycles 1 A g^{-1}	1 M H_2SO_4	[123]
Whisker	Ni–Co hydroxides	Hydrothermal	918.9 F g^{-1} 0.2 A g^{-1}	98.7% 3,000 cycles 2 A g^{-1}	6 M KOH	[124]
Caterpillar	$NiCo_2S_4$ on NF	hydrothermal /sulfurization	1,777 F g^{-1} 1 A g^{-1}	83% 3,000 cycles 10 A g^{-1}	5 M KOH	[126]
Caterpillar	PANI/P_4VP-g-GMWCNT	Chemical polymerization	1,065 F g^{-1} 0.5 A g^{-1}	92.2% 1,000 cycles 1 A g^{-1}	0.5 M Na_2SO_4	[127]
Worm	$NiMoO_4$ on carbon nanofiber	Hydrothermal	1,088.5 F g^{-1} 1 A g^{-1}	73.9% 5,000 cycles 10 A g^{-1}	2 M KOH	[130]
Worm	Ni–Co–P on NF	Electroless electrolytic deposition	222.16 F g^{-1} 1 mV s^{-1}	105% 1,000 cycles 50 mV s^{-1}	6 M KOH	[132]
Worm	N,S–carbon	Carbonization	456 F g^{-1} 0.3 A g^{-1}	NA	1 M H_2SO_4	[82]
Plume	Ni_3S_2 on rGO-NF	Hydrothermal	1462 F g^{-1} 1 A g^{-1}	93.% 2,000 cycles 1 A g^{-1}	2 M KOH	[133]
Nest	N, P-co-doped carbon	Microwave-assisted solvothermal method	171 F g^{-1} 0.2 A g^{-1}	96.2% 5000 cycles 2 A g^{-1}	6 M KOH	[83]
Nest	Fe:MnO_2	Electrodeposition	273 F g^{-1} 5 mV s^{-1}	92% 1,000 cycles 100 mV s^{-1}	1 M Na_2SO_4	[135]
Nest	N-doped carbon–V_3O_7	Hydrothermal, in situ photopolymerization method	660.63 F g^{-1} 0.5 A g^{-1}	80.47% 4,000 cycles 10 A g^{-1}	1 M Na_2SO_4	[137]
Ant-nest	$NiMoO_4$/carbonized melamine sponge	Carbonization/solvothermal	1,689 F g^{-1} 1 A g^{-1}	86.7% 5,000 cycles 10 A g^{-1}	3 M KOH	[140]
Ant-nest	MnO_2/carbon	Annealing, simple mixing	662 F g^{-1} 1 A g^{-1}	93.4% 5,000 cycles 1 A g^{-1}	6 M KOH	[142]

step to obtain 3D honeycomb-like porous carbon (HPC) foam nanostructure. The interconnected HPC (Fig. 2e) electrode material exhibited high surface area and was used for symmetric supercapacitor (SSC) device. The SSC device exhibited superior energy and power densities than reported carbon-based SSC devices as shown in Fig. 2f [77, 99, 103, 104]. In addition to that, various number of honeycomb-like structure have been reported for SC applications, confirming the importance of unique structure for energy storage applications. Table 2 shows the reported honeycomb-like structures.

2.1.2 Spider Web-Like Structure

Nature has always motivated and inspired human being for the fabrication of interesting and attractive nanostructures-based electrode materials [105– 107]. Both materials properties and determination of architectures are important for variety of applications [108, 109]. Spider webs are commonly found anywhere – at parks or even at homes. Spider webs are made from silk known for its exceptional toughness and flexibility, and water resistivity. Inspired by these characteristics, Deng et al. [110, 111] prepared

https://doi.org/10.1007/s40820-022-00944-z

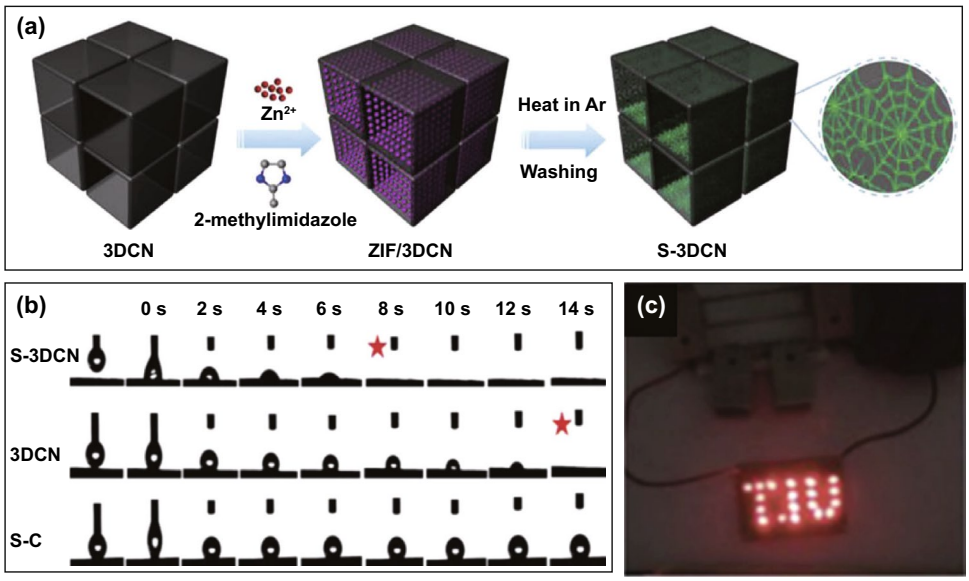

Fig. 3 **a** The illustrated scheme of the synthesis process, **b** The results of water-drop experiments of S-3DCN, 3DCN, and S-C, and **c** LED light devices powered by three supercapacitors connected in series. Reproduced with permission from Ref. [110]. Copyright 2018 Elsevier

a special design structure for energy storage device with exceptional mass transfer abilities. Figure 3a shows the schematic diagram of the preparation of 3D carbon network (3DCN) with bionic surface using zeolitic imidazolate frameworks (ZIF) as precursors. ZIF-8 polyhedron on carbon surface were connected to each other, forming spider web network-like structure. After annealing at 800 °C in argon for 2 h, the desired structure was achieved by washing away ZIF-8 with HCl and retaining 3D carbon network with "spider web"-like carbon, S-3DCN. The detailed mass transfer abilities for all three samples are given in Fig. 3b. Herein, S-3DCN portrayed a full adsorption of water drop at 8 s, out-performing 3DCN (14 s) and S-C (> 14 s), depicting S-3DCN has the best transportation ability. The as-prepared electrode material was further considered for energy storage applications and the solid-state SSC device (S-3DCN//S-3DCN) was fabricated. The nature-inspired S-3DCN spider web-like microstructures show multiple active sites toward electrolyte, numerous pores, excellent wettability of electrolyte. The designed SSC device successfully illuminated 19 LEDs as shown in Fig. 3c, which confirmed the advantaged of S-3DCN materials toward multiple applications.

The construction and design of 1D nanoarchitecture and the flexibility of binder-free electrode material have shown great interest for electrode fabrication. The practical

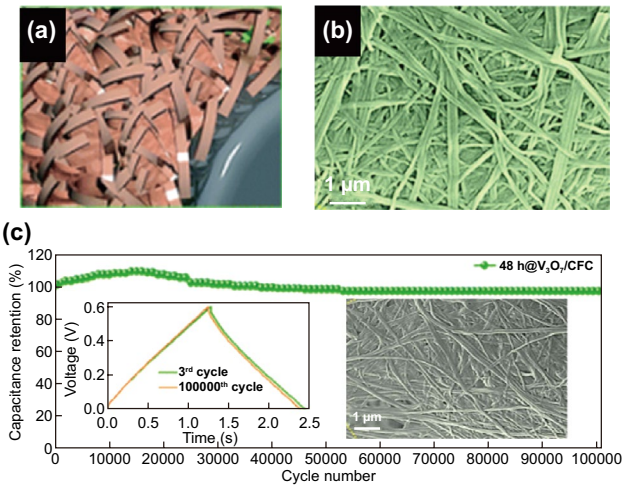

Fig. 4 **a** Schematic representation of the in situ growth of V_3O_7 spider web-like nanowires, **b** SEM image V_3O_7/CFC substrates. **c** Cycling stability of V_3O_7/CFC SSCs devices at a constant current density of 10 A g^{-1} for 100,000 cycles. Reproduced with permission from Ref. [118]. Copyright 2018, Royal Society of Chemistry

capacitance and stability of the metal oxide greatly depend on the composition, synthesis condition, and morphology of the structure [43, 63, 112, 113, 114, 115, 116, 117]. Manikandan et al. [118] designed binder-free vanadium oxide spider web-like nanostructure by using facile in situ hydrothermal technique for SSC devices. Figure 4a-b shows the

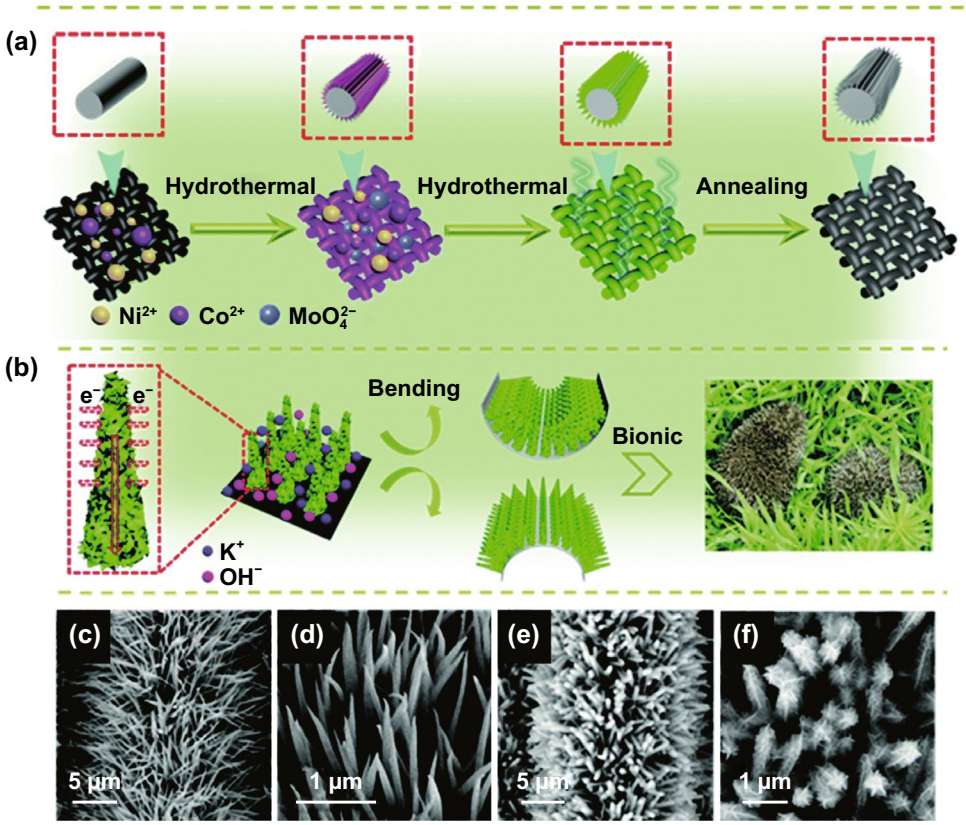

Fig. 5 **a** Schematic illustrations of $NiCo_2O_4$@$Ni_xCo_yMoO_4$ nanostructures (carbon fabric (black), $NiCo_2O_4$ nanoneedle clusters (pink), the $NiCo_2O_4$@$Ni_xCo_yMoO_4$ precursor (green), $NiCo_2O_4$@$Ni_xCo_yMoO_4$ (gray)); **b** charge transport and stress release in these hedgehog-like nanoneedle-cluster nanostructures; **c, d** SEM images of $NiCo_2O_4$ nanoneedle clusters; and **e, f** $NiCo_2O_4$@$Ni_xCo_yMoO_4$ nanostructures. Reproduced with permission from Ref. [119]. Copyright 2018, Royal Society of Chemistry

schematic diagram and the scanning electron microscopy (SEM) image of the as-synthesized spider web-like structure. The nature-inspired based SSC device exhibited exceptional stability of 97% after 100,000 cycles (Fig. 4c). Even after 100,000 cycles, the spider web-inspired nanostructure was preserved as shown in the inset of Fig. 4c.

2.1.3 Hedgehog Quills Structure

Hedgehogs are unique pets that have spines consisting of hollow hairs. These spines, called as quills, can be curled, or straightened upon muscle control. Inspired by the curling up and relaxation of their quills and the exterior structure of hedgehogs, researchers have utilized these structures to cater an electrode's architecture for SC application [119, 120, 121]. Sun et al. [119] reported of hedgehog-inspired electrode material for flexible SC devices. Figure 5a shows the preparation of $NiCo_2O_4$@$Ni_xCo_yMoO_4$ core–shell hedgehog-like nanoneedle-clusters nanostructures. The synthesis was done in two-step facile hydrothermal method. In the first step, carbon fabric was used as a current collector and a substrate to grow $NiCo_2O_4$ hedgehog-like nanoneedles with a maximum diameter of 150 nm (Fig. 5c-d). In the second step, $Ni_xCo_yMoO_4$ nanosheets were wrapped on the initially prepared $NiCo_2O_4$ nanoneedle clusters, forming $NiCo_2O_4$@$Ni_xCo_yMoO_4$ core–shell hedgehog-like nanoneedle-cluster nanostructures (Fig. 5e-f). Figure 5b shows the utilization of the hedgehog-like structure for charge transport and stress release mechanism. Such combination of nanosheets grown on nanoneedles may be beneficial in giving sufficient space between the active materials which can provide better electrolyte infiltration and plentiful electroactive sites for redox reaction. The as-assembled all-solid-state flexible battery-type hybrid supercapacitor (HSC), $NiCo_2O_4$@$Ni_xCo_yMoO_4$//AC, demonstrated outstanding outcomes with a high

 https://doi.org/10.1007/s40820-022-00944-z

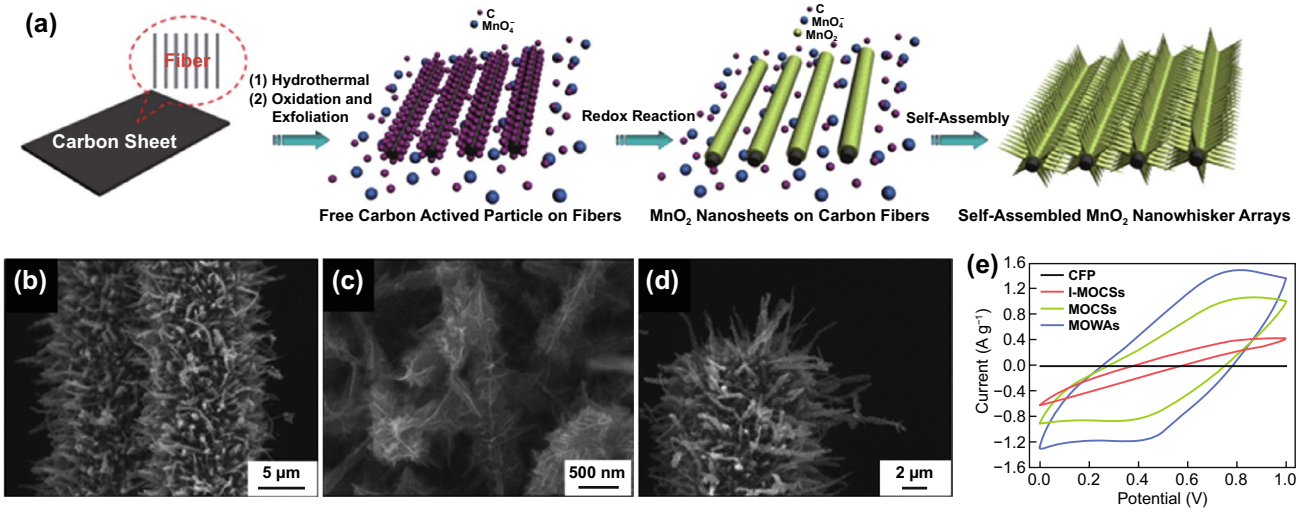

Fig. 6 **a** Schematic illustration for the formation processes, (**b**–**d**) SEM images of the MOWAs, and **e** CV curves of the different electrode materials at 50 mV s^{-1}. Reproduced with permission from Ref. [122]. Copyright 2012, Royal Society of Chemistry

specific capacitance of 207 F g^{-1} (1 A g^{-1}) a high energy density (64.7 Wh kg^{-1} at 749.6 W kg^{-1}) and promising cycling stability (nearly 100% after 10,000 cycles).

2.1.4 Whisker-Like Structures

Luo et al. [122] synthesized self-assembled whisker-like MnO_2 arrays on carbon fiber paper (MOWAs) using simple in situ redox replacement reaction in a hydrothermal method (Fig. 6a). In their study, different amount (3–15 mM) of potassium permanganate ($KMnO_4$) was used as precursor to MnO_2 yielding to different morphologies. At 7 mM $KMnO_4$, highly ordered whisker-like MnO_2 arrays are consistently observed covering the whole carbon fiber (Fig. 6b). At a higher magnification (Fig. 6c), each whisker is made up of many interconnected and ultrathin nanosheets. An individual MOWA is shown in Fig. 6d portraying a length of 3–5 μm and about 0.5 μm in diameter at the middle section. Other morphologies were also observed upon changing $KMnO_4$'s concentration to 3 mM (carbon fiber/MnO_2 core–shell nanostructures, MOCSs) and 15 mM (ill-defined carbon fiber/MnO_2 core–shell nanostructures, I-MOCSs). Figure 6e shows a comparative study of the cyclic voltammetry (CV) curves of carbon fiber paper (CFP), MOWAs, as well as the two other prepared structures, MOCs and I-MOCs. Among all electrodes, MOWAs exhibited the largest CV curve. The specific capacitance obtained for MOWAs electrode at 100 mA g^{-1} is 274.1 F g^{-1}. The long-term cycling stability of MOWAs electrode resulted in a retention of 95% after 5,000 cycles (100 mA g^{-1}). With such unique structure of small MnO_2 sheets directly attached on CFP, MOWAs' architecture provided well separated yet conductive sheets that paved way for better ion insertion and transport. Other whisker-like structured electrodes are reported in polyaniline on carbon nanofiber (CNF) [123], floss-like Ni–Co binary hydroxide composites assembled with whisker-like nanowires [124], and polyaniline (PANI) whiskers [125].

2.1.5 Caterpillar and Worm-Like Structures

Caterpillars and worms are both cold-blooded species typically with a long tube-like body. However, worms consist of smooth-structured body that do not have legs, eyes nor hair. In contrast, caterpillars have segmented bodies which appears to be rough and hairy. In a nanostructure level, caterpillar-like and worm-like structures have been investigated in SC applications. For instance, caterpillar-like $NiCo_2S_4$ nanocrystal arrays on nanofibers (NF) [126] and polyaniline/CNT hybrids with core–shell structures [127] are successfully synthesized as electrode materials. Figure 7a shows the SEM image of the $NiCo_2S_4$ nanosheet@nanowires (NSNW) which exhibits a caterpillar-like structure [126]. The $NiCo_2O_4$ consists of vertical nanosheets aligned on NF with each sheet having multidirectional nanowires. Figure 7b

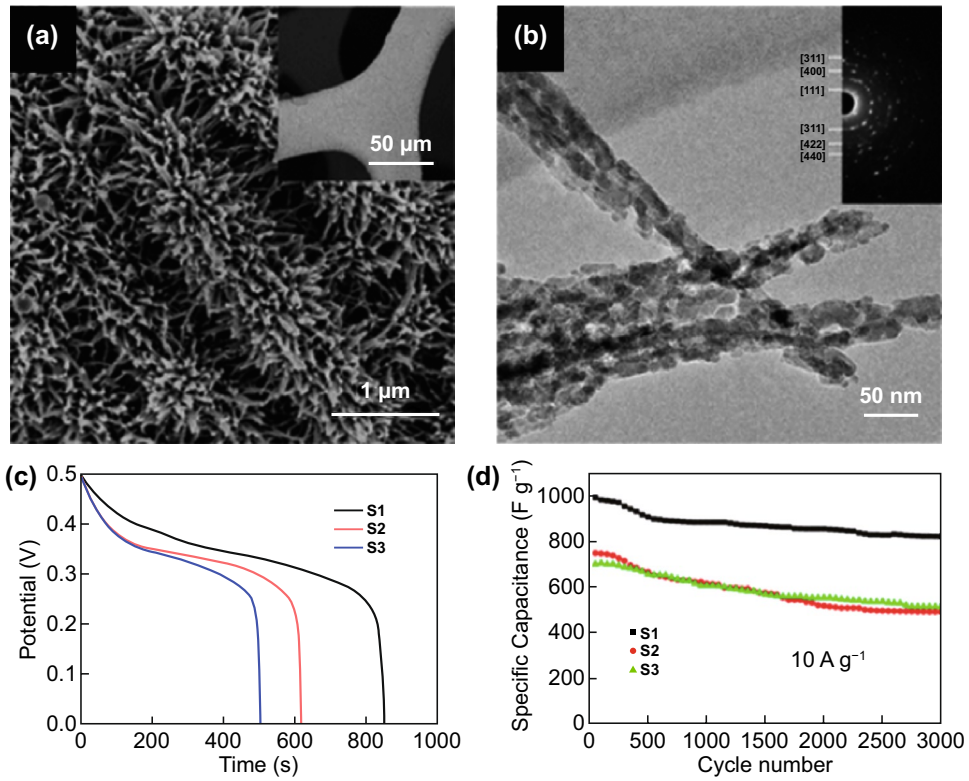

Fig. 7 **a** SEM images of $NiCo_2S_4$/NF. **b** TEM image of nanowires from $NiCo_2S_4$ NSNWs; the inset in (b) shows SAED pattern, **c** GCD curves at 1 A g^{-1}, and **d** Stability at 10 A g^{-1} of the S1, S2, and S3 electrodes. Reproduced with permission from Ref. [126]. Copyright 2017, ACS Publications

shows a transmission electron microscopy (TEM) image of the nanowire with a dimension of bottom core ~50 nm and a tip ~30 nm. Aside from the caterpillar-like $NiCo_2S_4$ NSNW structures, other structures were prepared by varying the time of maintained reaction. The sealed autoclave maintained at 95 °C for 12, 10, and 8 h yielded the Ni–Co precursor NSNWs, Ni–Co precursor NSNP, and Ni–Co precursor NS, respectively. The difference in morphologies and its effect in electrochemical performance were evaluated and the discharge curves are shown in Fig. 7c. $NiCo_2S_4$ nanosheet@nanowires (NSNW, S1), $NiCo_2S_4$ nanosheet@nanoparticles (NSNP, S2), and $NiCo_2S_4$ porous nanosheets (NS, S3) and their specific capacitances are 1,777, 1,238, and 1,010 F g^{-1}, respectively, at the same current density of 1 A g^{-1}. The caterpillar-like structure also benefited the S1 electrode with a retention of 83% after 3,000 cycles (10 A g^{-1}), compared with S2 (66%) and S3 (73%) (Fig. 7d).

Worm-like structures have been prepared in N-doped graphitized porous carbon [128], mesoporous carbon [129], $NiMoO_4$ coaxially decorated on electro-spun CNF [130], amorphous MnO_2 nanowires grown on textiles [131], Ni–Co–P deposited on NF [132], and N/S-co-doped porous carbon [82]. Figure 8a shows the SEM image of a nitrogen-doped worm-like hierarchical porous carbon with graphitized porous carbon embossment (NWHC-GE), which was prepared by polymerization-induced colloid aggregation method followed by coordination–pyrolysis process [128]. The worm-like structure was likely plausible due to the presence of ferrous sulfate heptahydrate (FSH) as a precursor. Aside from the worm-like structure formed from the addition of 0.01 mol FSH in the material preparation, the key influence of FSH leads to formation of other structures, such as N-doped hollow carbon sphere (NHCS, no FSH was added) and N-doped hollow carbon capsule (NHCC, 0.02 mol FSH was added). Figure 8b shows a comparative GCD profiles of NHCS, NWHC-GE, and NHCC at a current density of 20 A g^{-1} portraying the longest GCD curved favorable to NWHC-GE. At 1 A g^{-1}, the higher specific capacitance of NWHC-GE is 178 F $g^{-1}$is attained compared to NHCS (114 F g^{-1}) and NHCC (156 F g^{-1}). A better electrical conductivity and

 https://doi.org/10.1007/s40820-022-00944-z

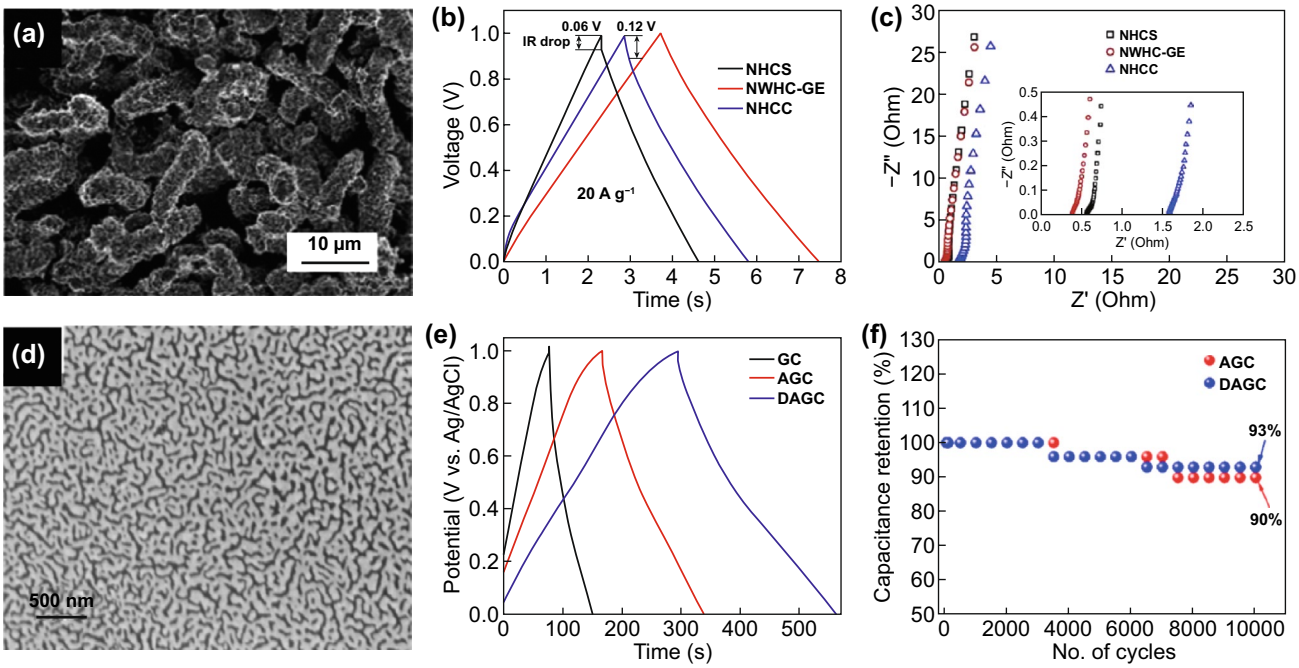

Fig. 8 **a** SEM images of NWHC-GE before heat treatment; comparison of (**b**) GCD curves at 20 A g^{-1}, and **c** Nyquist plot for different electrodes. Reproduced with permission from Ref. [128]. Copyright 2017, Elsevier. **d** SEM image of DAGC sheets; **e** comparison of (b) GCD curves at 1 A g^{-1}, and **f** Stability test for different electrodes. Reproduced with permission from Ref. [82]. Copyright 2020, Elsevier

lower resistivity were also observed for NWHC-GE (0.39 Ω) than that of NHCS (0.57 Ω) and NHCC (1.58 Ω) (Fig. 8c). Such improved performance is credited to a higher graphitization degree and an optimized nitrogen-doping content for NWHC-GE.

Similarly, Gopalakrishnan et al. [82] reported worm-like hierarchical structures based on nitrogen, sulfur-co-doped porous carbon were derived from ginger. Inspired by ginger as biomass source for carbon, ginger was pre-activated using NaCl/KCl followed by carbonization (800 °C) and removal of salt ions through washing with diluted HCl (product denoted as AGC). To dope AGC with nitrogen and sulfur, thiourea was used as precursor and went under another carbonization (800 °C) (product denoted as DAGC). The final structure of the doped & activated ginger carbon (DAGC) with unique worm-like pore structure and interconnected cavities is shown in Fig. 8d. The worm-like structure not only gained a high specific surface area (720 m^2 g^{-1}) but also yielded to an improved electrochemical performance. Figure 8e shows a comparative GCD curves for DAGC, AGC (activated ginger-derived carbon), and GC (ginger-derived carbon without any activation and doping). Clearly, DAGC showed a lengthy charge and discharge profiles which can be acquainted to a better ion storage and high capacitive performance. The highest performance conducted at 1 A g^{-1} was obtained for DAGC (268 F g^{-1}) compared to GC (75 F g^{-1}) and AGC (172 F g^{-1}). The stability for GC and DAGC were compared at constant current density (Fig. 8f). The superior electrochemical performance can be acquainted to DAGC's thin carbon nanosheets morphology with worm-like pore structures and heteroatom doping, which utilized rapid ion transfers and maximum charge storage capacity [73, 74, 75].

2.1.6 Plume-Like Structure

A plume is similar to a structure of a bird's feather that consists of tiny hair-like strands. Jinlong et al. [133] initially deposited graphene oxide (GO) sheets on NF by dipping in a GO dispersion and thermal reduction annealing. Then, Ni_3S_2 was grown by hydrothermal method on the pre-deposited GO on NF. The final resulting structure is a plume-like Ni_3S_2 grown on the NF with thermal reduced graphene oxide (rGO) architecture as shown in Fig. 9a. Figure 9b shows the CV curve representing the electrochemical performance

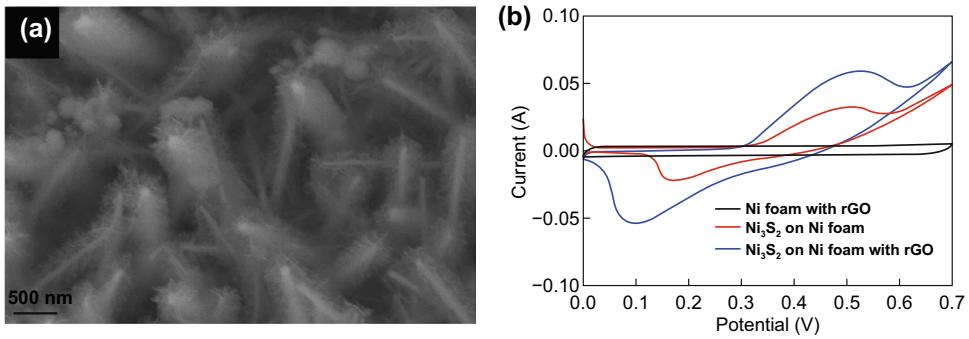

Fig. 9 **a** SEM image plume-like structure and **b** comparison of CV curves plume-like structure compared to rGO on NF and Ni_3S_2. Reproduced with permission from Ref. [133]. Copyright 2017, Elsevier

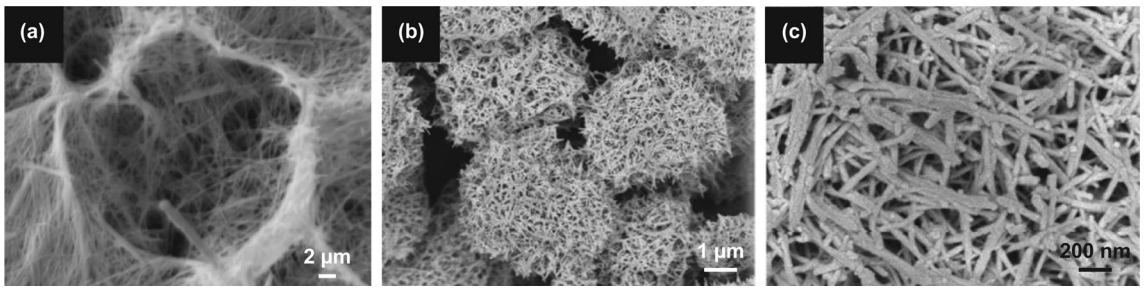

Fig. 10 **a** SEM image of nest-like The $Ni@Ni_{1.4}Co_{1.6}S_2$. Reproduced with permission from Ref. [138]. Copyright 2015, Royal Society of Chemistry. **b-c** SEM image of nest-like structures based from MnO_2. Reproduced with permission from Ref. [139]. Copyright 2013, Elsevier

of the plume-like structure compared to rGO on NF and Ni_3S_2 on NF only. At a scan rate of 2 mV s^{-1}, larger non-rectangular CV curves were observed for the Ni_3S_2 on NF with rGO electrode. The plume-like structured electrode delivered a high capacitance of 1,462 F g^{-1} (1 A g^{-1}) and retained 98.34% of its capacitance on the first 1,000 cycles. The plume-like Ni_3S_2 on NF with rGO exhibited better SC performance and improved cycling stability which is valuable for energy storage applications.

2.1.7 Nest-Like Structures

By nature, nests are built by animals, such as birds, to hold their eggs and to serve as a home for the young ones. Bird's nest comprises of dried leaves, branch, or grasses that is coiled into a cup-shape. Nest-like architectures are studied and structured in electrode materials, such as N- and P-co-doped mesoporous carbon [83], glucose-derived nitrogen-doped hollow carbon [134], Fe-doped MnO_2 [135], polyaniline [136], and V_3O_7 [137]. A nest-like structure based on $Ni@Ni_{1.4}Co_{1.6}S_2$ [138], MnO, and V_3O_7 [137] are shown in Fig. 10. Mi et al. [138] initially synthesized $Ni@Ni_3S_2$ with a nest-like structure. $Ni@Ni_{1.4}Co_{1.6}S_2$ was then synthesized by a Co-exchange method by using $Ni@Ni_3S_2$ as a template. The $Ni@Ni_{1.4}Co_{1.6}S_2$ is composed of a network of nanowires which forms numerous micro-/nanoholes mimicking a nest (Fig. 10a). With a similar structure yet with the addition of Co-ions, the specific capacitance of $Ni@Ni_{1.4}Co_{1.6}S_2$ is 122 F g^{-1}, compared to $Ni@Ni_3S_2$ (89 F g^{-1}) at 1 A g^{-1}. Figure 10b shows a bird's nest-like structures based on MnO_2 [139]. The self-organized structure formed clusters with ~ 4–5 μm diameter consisting of interconnected nanowires (Fig. 10c). With such organized structure, the maximum specific capacitance of 917 F g^{-1} at a current density of 5 mA cm^{-2} was obtained.

Another nest-like structure is based on the home of ants or anthills. Anthills are commonly built underground. Inside an anthill is a massive network of interior channels and chambers. Inspired by such unique interconnected structure, ant-nest-based nanostructures have been utilized as electrode materials. A unique ant-nest-like structured electrode was prepared in $NiMoO_4$/ carbonized melamine sponge (CMS) using solvothermal reaction (Fig. 11a) [140]. $NiMoO_4$

 https://doi.org/10.1007/s40820-022-00944-z

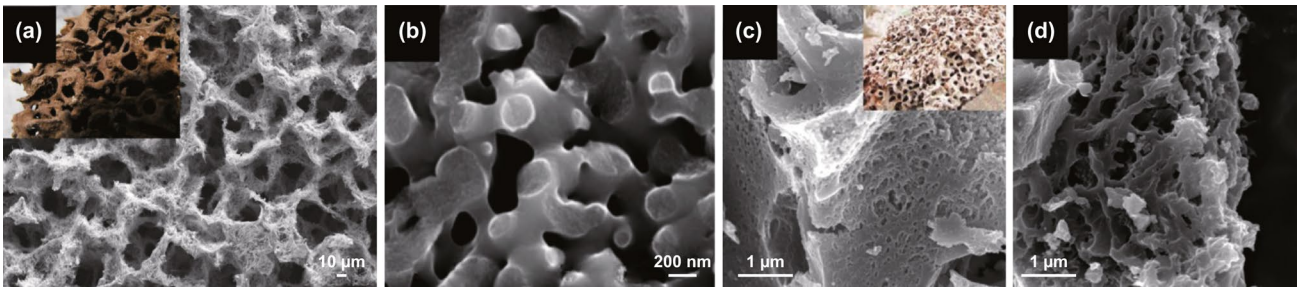

Fig. 11 **a** SEM image of ant-nest-like $NiMoO_4$/CMS, inset is ant-nest. Reproduced with permission from Ref. [140]. Copyright 2018, Royal Society of Chemistry. **b** SEM image of carbon-based ant-nest-like structures. Reproduced with permission from Ref. [141]. Copyright 2019, Wiley. **c** SEM image of ant-nest-like ANHPC and **d** SEM image MnO_2/ANHPC. Reproduced with permission from Ref. [142]. Copyright 2018, ACS Publications

nanorods are grown on the CMS by solvothermal reaction while maintaining the interconnected channels of CMS sponge. The optimized $NiMoO_4$/CMS electrode exhibited a high specific capacitance of 1,689 F g^{-1} (1 A g^{-1}). Miao et al. [141] studied carbon-based ant-nest-like structures are prepared using NF supported hierarchical porous carbon (NF-HPC). A 3D crossed-linked and associated backbones (diameter of ≈200 nm) aided the formation of highly uniform and well-interconnected porous structure (Fig. 11b). As a symmetric SC device, the outstanding electrochemical performance of the device resulted in a high specific capacitance (292 at 0.25 A g^{-1}) and long-term cycling stability (100% at 5 A g^{-1} after 30,000 cycles). Lastly, a unique 3D ant-nest-like hierarchical porous carbon (ANHPC) is shown in Fig. 11c [142]. The ant-nest-like structure of ANHPC possesses large surface area (2,372 m^2 g^{-1}) and high pore volume (1.936 m^3 g^{-1}. The exceptional structure was then utilized to embed MnO_2 and obtain MnO_2/ANHPC composites (Fig. 11d). It is clearly observed that the carbon skeleton structure has not collapsed and retained the structure of ANHPC. The ant-nest-inspired structures give a favorable architecture for rapid ion transfer/diffusion. The combination of EDLC-based ANHPC and pseudocapacitance-based MnO_2 yielded to a high specific capacitance of 662 F g^{-1} at 1 A g^{-1} compared to ANHPC at 254 F g^{-1}. The detailed electrochemical performance of animal-inspired structure tabulated in Table 2.

2.2 Human Body-Inspired Structures

2.2.1 Spine-Like Structure

Park et al. [84] prepared spine-like nanostructured carbon interconnected by graphene with SC applications. The preparation of spine-like graphene-interconnected nanostructured carbon consists of three steps: i) preparation of platelet-type CNF (P-CNF) by chemical vapor deposition (CVD), ii) an expanding process by oxidation treatment, and iii) a co-solvent exfoliation method and reduction processes. Figure 12a-b shows the SEM and TEM image of the spine-like nanostructured carbon which is composed of regularly occurring intervals of exfoliated graphitic blocks and graphene nanoplatelets. In a three-electrode system, the spine-like nanostructured carbon exhibited significantly improved electrochemical performance (272 F g^{-1} at 10 mV s^{-1}) compared to as-prepared P-CNF (19 F g^{-1}) (Fig. 12c). To further use into practical application, the two-electrode system delivered a high capacitance (238.8 F g^{-1} at 2.5 A g^{-1}), rate capability (230 F g^{-1} at 200 mV s^{-1}, above 85% of the initial value at 10 mV s^{-1}), and cycle stability (94% after 3,000 cycles) for the spine-like nanostructured carbon (Fig. 12d).

2.2.2 Finger-Like Structure

Finger-like structures are used as effective designs for electrode materials in multifunctional integrated micro/nano systems [152, 153, 154, 155, 156]. In-plane finger-like structures are advantageous for micro-supercapacitors for it provides suitable accessibility for ion transport as the edges of the active electrodes are exposed to the electrolyte. Also, the finger-like design eliminates the use of separators as needed in conventional sandwich structures of SCs which also decreases the resistance and leads to high-frequency response as the distance between the electrode finger arrays is small [157]. Wang et al. [158] fabricated

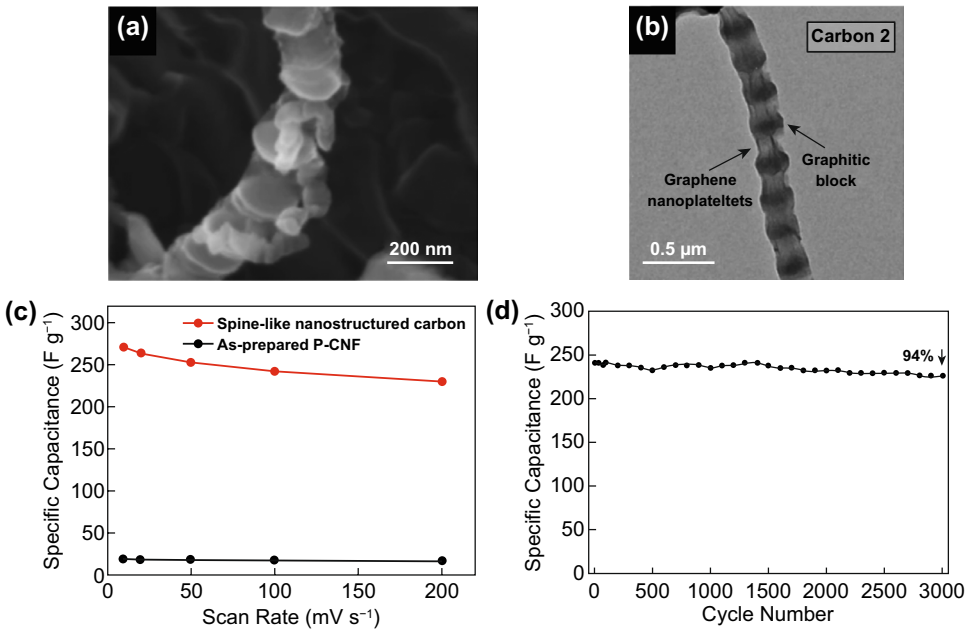

Fig. 12 **a-b** SEM and TEM of spine-like nanostructured carbon, **c** rate capabilities of as-prepared P-CNF and spine-like nanostructured carbon, **d** cycle stability of the spine-like nanostructured carbon measured at a scan rate of 100 mV s^{-1}. Reproduced with permission from Ref. [84]. Copyright 2014, Nature publisher

vertical finger-like asymmetric supercapacitors (VFASCs) comprising of rGO–manganese dioxide–polypyrrole (rGO-MnO_2-PPy) as positive electrode and RGO–molybdenum trioxide (rGO–MoO_3) as negative electrode. Various mass loading was investigated with structures mimicking 2 to 10 finger-like electrodes (Fig. 13a). The CV (Fig. 13b) and GCD (Fig. 13c) curves showed the highest performance for the 10 finger-like electrodes ($5m_0$). The specific capacitance increased with the increased of mass loading (Fig. 13d) with $5m_0$ recording the highest capacitance of 31.4 F g^{-1} (34.8 F cm^{-3}). The $5m_0$ electrode showed a high energy density of 12.94 mW h cm^{-3} (power density at 0.47 W cm^{-3}) and still maintained the high value of 2.59 mW h cm^{-3} (power density at 3.72 W cm^{-3}) with 88.2% capacitance retained after 10,000 cycles (Fig. 13e-f). For practical application, bending experiment was done to show the flexibility of the electrode as shown in Fig. 13g. Moreover, two electrodes connected in series accumulating 3.2 V were successful in lighting two LEDs (Fig. 13h).

2.2.3 DNA-Like Structure

Another fascinating nature-inspired nanoarchitecture is a double helical DNA-like WO_{3-x}/C microfiber superstructure [159]. Salkar et al. [159] prepared a self-assembly of in situ carbon fiber encapsulated by WO_{3-x}/C nanorods depicting a DNA-like structure as shown in Fig. 14a. The double helical DNA-inspired assembly provides favored structure allowing better participation of ions during electrochemical reaction. Figure 14b shows the CV curves with different scan rate (25 to 250 mV s^{-1}) across the − 0.5 to 0.3 V potential range. At 25 mV s^{-1}, the specific capacitance is 169.2 F g^{-1}. Using the GCD curves, the highest specific capacitance was recorded at 498.4 F g^{-1} at 1.2 A g^{-1} (equivalent to areal capacitance of 401.4 mF cm^{-2} at 2 mA cm^{-2}) (Fig. 14c). A solid-state asymmetric supercapacitor (ASC) device was assembled a deliver a power density of 498 W kg^{-1} at an energy density of 15.4 Wh kg^{-1}. The rare DNA-like morphology only justified its unusual yet important structure in the development of electrode nanoarchitectures.

2.2.4 Dendrite-Like Structure

Dendrites are pronged extensions of a nerve cell which is similar to a tree-like structures. Dendrite formation has also been observed in mineral crystal growth, as well as, in snowflake and frost pattern formations. These unique structures have been observed in the growth of Au

 https://doi.org/10.1007/s40820-022-00944-z

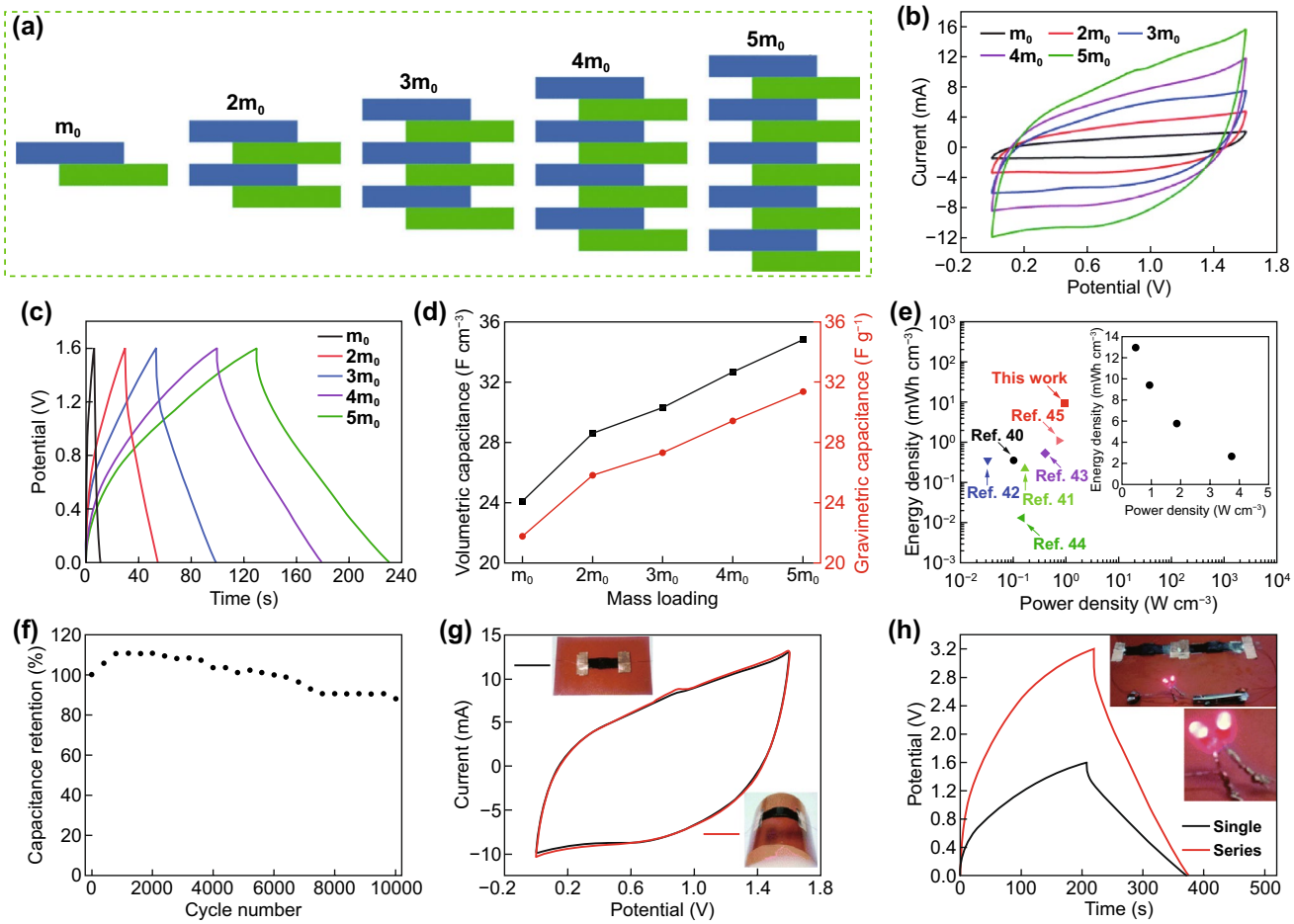

Fig. 13 Electrochemical performances and applications of VFASCs. **a** Schematic diagram, **b** CV curves at a scan rate of 20 mV s^{-1}, **c** GCD curves, and **d** volumetric capacitances and gravimetric capacitances with various mass loadings of the VFASCs. **e** Energy and power density plot and **f** cycle life of the VFASCs with a mass loading of $5m_0$. **g** CV curves of the finger-like ASCs in the straight and bent states. **h** GCD curves of a single and two finger-like supercapacitors connected in series. The inset shows two lit LED lamps powered by the two VFASCs in series. Reproduced with permission from Ref. [158]. Copyright 2017, Royal Society of Chemistry

dendrites containing long back bone stems with several branches and highly corrugated structures [160], Co_3O_4 nanostructure made up of nanorods [161], and dendrite-like MnO_2 nanostructures grown on carbon cloth [162]. Figure 15 shows the synthesis of MnO_2 nanowires grown on hollow Ni dendrites prepared by Sun et al. [163]. Initially, Cu dendrites were first prepared on Ni substrate using electrodeposition (Fig. 15a, e–g). The as-formed Cu dendrites were then coated with a thin layer of Ni using electroplating (Cu@Ni) (Fig. 15b). Then, Cu was selectively removed from Cu@Ni through anodic dissolution, leaving a hollow Ni (Fig. 15c, h-j). Finally, Ni@MnO_2 was prepared by growing MnO_2 nanowires on the surface of hollow Ni using anodic pulse electrochemical deposition (Fig. 15d, k-m). When applied as an electrode, the Ni@MnO_2 electrode delivered a specific capacitance of 1125 F g^{-1} (5 mV s^{-1}) at a MnO_2 mass loading of 0.35 mg cm^{-2}. When a higher MnO_2 mass loading was increased to 1.8 mg cm^{-2}, the specific capacitance resulted in 303 F g^{-1} (5 mV s^{-1}). The outstanding electrochemical performance of the Ni@MnO_2 electrode can be attributed to the following nanoarchitecture: first, the highly conductive hollow Ni dendrites acted as both support and current collector that allowed the pathway for fast electron transport; second, the MnO_2 nanowire arrays permitted productive material utilization; lastly, the existence of hierarchical porous channels in the overall construction facilitates fast diffusion between the electrode and electrolyte [39, 40,

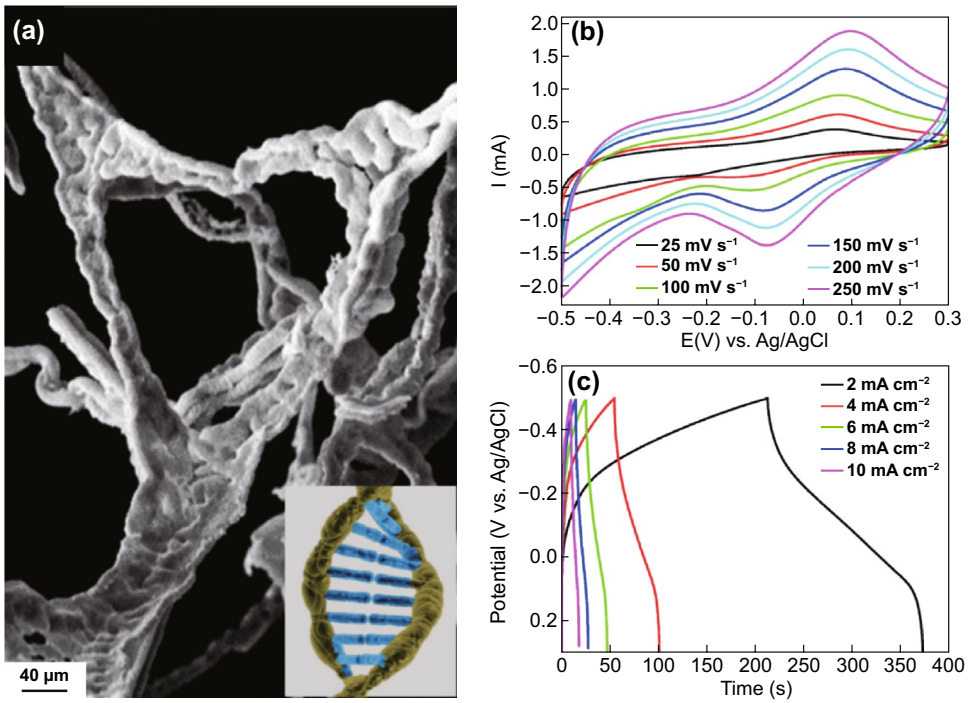

Fig. 14 **a** SEM image depicting DNA-like double helical tripodal microfiber superstructure along with representative DNA image shown in the inset for comparison. **b** Scan rate-dependent CV curves and **c** GCD curves at different current densities for DNA-like double helical WO_{3-x}/C microfibers. Reproduced with permission from Ref. [159]. Copyright 2020, ACS Publications

47, 48, 56, 164, 165]. The detailed electrochemical performance of human-inspired structure tabulated in Table 3.

3 Future Outlooks and Conclusion

In this review article, we have highlighted the importance of animal and human body-inspired materials down to the nanoscale level for SC application. Materials with different dimensionalities can be fabricated, tailored, and exploited according to several factors to construct nature-inspired formation of interconnected and hierarchical nanostructures. It is interesting to note that such dimensional structures can generate ordered structures, which are highly valued as the electrode materials. Still, the overall electrochemical performance will matter for practical use. Though having a high capacitance and capacitive property is highly desirable for many electrodes that has been researched, it is only one of the important properties that must be considered in constructing electrode materials. Nevertheless, a lot of hindrances have been assessed why scientifically studied electrodes cannot be launched in the market.

Nature-inspired materials with high porosity are found to be feasible for energy storage applications. The current article systematically summarized SC application of few of such nature-inspired materials. However, such materials also shave some drawbacks, which are enlisted below with future research directions.

1. Large scale production of such nature-inspired materials with cost-effectiveness is quite complicated. For example, metal precursors displayed considerable electrical and chemical properties. However, researchers must consider the long-term availability of these precious metals as well as their costs if they want to concentrate on producing metal-based electrode materials in commercial scale. Moreover, precise production of such material is also highly challenging. In this aspect, the 3D printing techniques have the ability to copy the natural structures. The printed products are also found to be highly flexible, which can be applicable for constructing flexible and stretchable supercapacitors. Therefore, future manufacturing of nature-inspired materials can be focused on these techniques for scalable production.
2. Apart from their structures and morphologies, other factors, like the nature of electrode materials, choice of

 https://doi.org/10.1007/s40820-022-00944-z

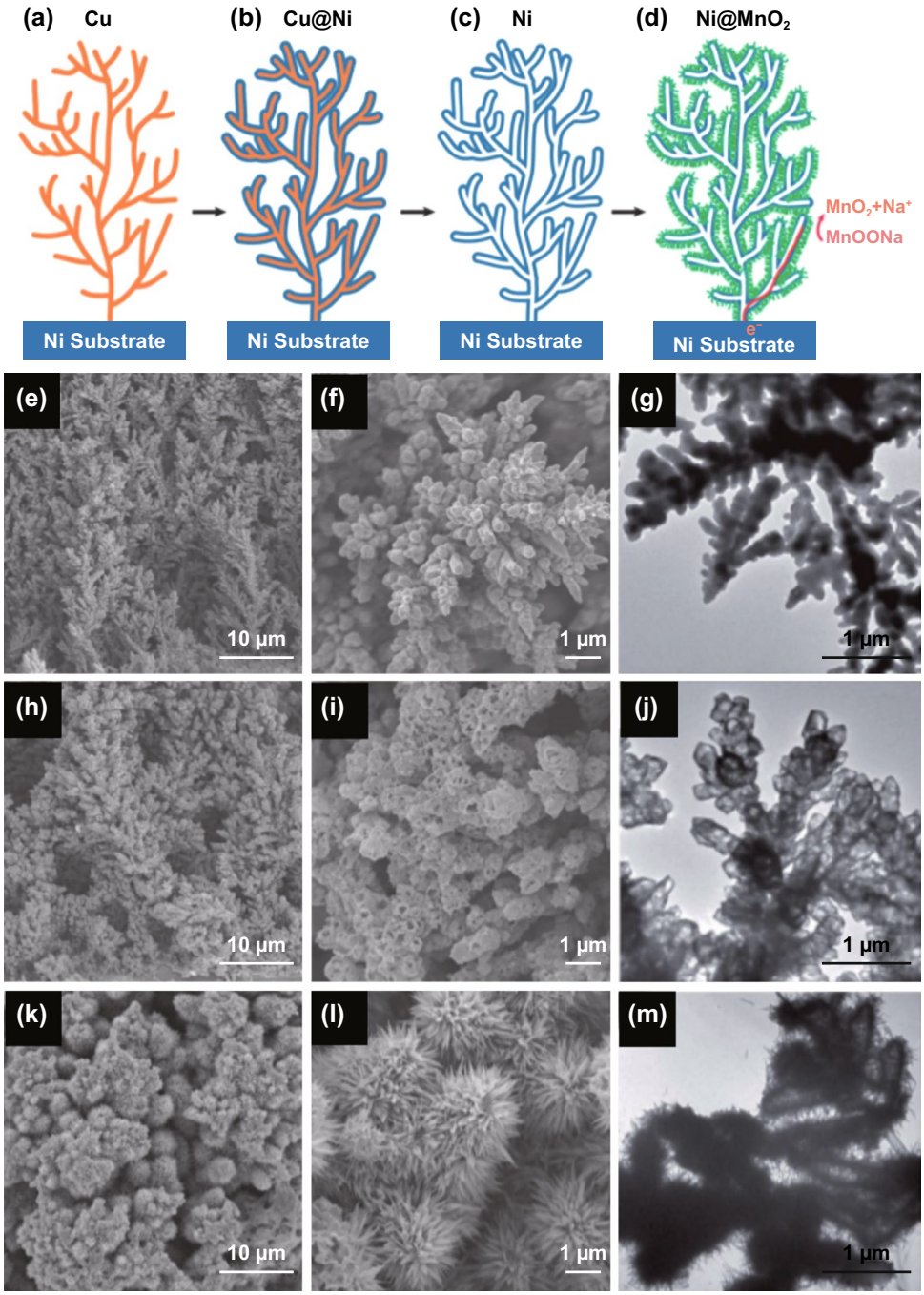

Fig. 15 Synthesis of MnO_2 nanowires supported on hollow Ni dendrites. **a** Electrodeposition of a nanoforest of Cu dendrites; **b** electroplating of Ni on Cu dendrites; **c** selective dissolution of Cu; **d** electrodeposition of MnO_2 nanowires on hollow Ni dendrites to form a hierarchical Ni@MnO_2 porous structure. SEM and TEM images of (**e**–**g**) Cu dendrites, **h**–**j** hollow Ni dendrites, and **k**–**m** Ni@MnO_2 structure, respectively. Reproduced with permission from Ref. [163]. Copyright 2013, Royal Society of Chemistry

electrolytes, use of binders, and nature of current collections, have also played significant role on the electrochemical performance of any electrode materials. Smart combination of EDLC-type and pseudocapacitive-type materials with nature-inspired structures is found to be a feasible strategy to improve the capacitive perfor-

Table 3 Comparison of human-inspired structures in three-electrode measurements

Electrode structure	Electrode materials	Method	Three-electrode measurements			Refs.
			Capacitance	Cycling stability	Electrolyte	
Human body-inspired structures						
Spine	Graphitic carbon	Co-solvent exfoliation	272 F g^{-1} 10 mV s^{-1}	94% 3,000 cycles 100 mV s^{-1}	1 M H_2SO_4	[84]
Finger	MoS_2	Spray painting, laser patterning	8 mF cm^{-2} or 178 F cm^{-3} 10 mV s^{-1}	~92% 1,000 cycles 0.22 A m^{-2}	1 M NaOH	[152]
Finger	MXene-MoS film	Laser engraving	75.5 F g^{-1} or 173.6 F cm^{-3} 1 mV s^{-1}	98% 6,000 cycles 0.335 A g^{-1}	2 M $ZnSO_4$	[153]
DNA	WO_{3-x}/carbon Fiber	Simple mixing/reflux	401 mF cm^{-2} 2 mA cm^{-2}	> 94% 5,000 cycles 8 mA cm^{-2}	0.5 M H_2SO_4	[159]
Dendrite	Co_3O_4	Hydrothermal	207.8 F g^{-1} 0.5 A g^{-1}	97.5% 1,000 cycles 1.8 A g^{-1}	3 M KOH	[161]
Dendrite	MnO_2 on carbon fiber cloth	Hydrothermal	430 F g^{-1} 1 A g^{-1}	82.75% 10,000 cycles 1 A g^{-1}	1 M Na_2SO_4	[162]
Dendritic	Ni@MnO_2	Electrodeposition	1125 F g^{-1} 5 mV s^{-1}	103% 1,000 cycles 12.5 A g^{-1}	1 M Na_2SO_4	[163]

mance. Although, such combination requires much more research attention for commercialization.

3. In-depth knowledge of the charge storage mechanism of such nature-inspired materials is highly required for future research. In this aspect, the in situ characterization techniques like in situ TEM, in situ XRD, in situ Raman spectra, in situ XPS, etc. can be a pivotal approach to incorporate in material characterization in order to better understand the physiochemical properties of the active materials.
4. It is evident that the electrochemical performance of such nature-inspired materials can be tuned by manipulating the interfacial interactions of individual components. However, detailed theoretical study is necessary in this topic.
5. Nature-inspired structures based on newly developed 2D materials like MXene should be explored for a wide variety of applications.
6. The differences in EDLC-, pseudocapacitive-, and battery-type electrode materials; symmetric, asymmetric, and hybrid SC devices; and the appropriate selection of potential/voltage window as well as suitable equations for the calculations of energy density should be carefully selected as previously discussed [21, 166, 167].

Acknowledgements This work was supported by the Donations for Research Projects_RMGS (project number 9229006). M.A.A. expresses appreciation to the Deanship of Scientific Research at King Khalid University Saudi Arabia (R.G.P. 2/40/43).

Funding Open access funding provided by Shanghai Jiao Tong University.

References

1. C. Xu, A.R. Puente-Santiago, D. Rodríguez-Padrón, M.J. Muñoz-Batista, M.A. Ahsan et al., Nature-inspired

hierarchical materials for sensing and energy storage applications. Chem. Soc. Rev. **50**(8), 4856–4871 (2021). https://doi.org/10.1039/C8CS00652K

2. Y. Liu, K. He, G. Chen, W.R. Leow, X. Chen, Nature-inspired structural materials for flexible electronic devices. Chem. Rev. **117**(20), 12893–12941 (2017). https://doi.org/10.1021/acs.chemrev.7b00291
3. Z.A. ALOthman, D. Rodriguez-Padron, R. Luque, A.M. Balu, Innovative nanomaterials for energy storage moving toward nature-inspired systems. Curr. Opinion Green Sustain. Chem. **32**, 1005 (2021). https://doi.org/10.1016/j.cogsc.2021.100520
4. C. Wan, Y. Jiao, D. Liang, Y. Wu, J. Li, A geologic architecture system-inspired micro-/nano-heterostructure design for high-performance energy storage. Adv. Energy Mater. **8**(33), 1802388 (2018). https://doi.org/10.1002/aenm.201802388
5. J. Tang, P. Yuan, C. Cai, Y. Fu, X. Ma, Combining nature-inspired, graphene-wrapped flexible electrodes with nanocomposite polymer electrolyte for asymmetric capacitive energy storage. Adv. Energy Mater. **6**(19), 1600813 (2016). https://doi.org/10.1002/aenm.201600813
6. N.S. Ha, G. Lu, a review of recent research on bio-inspired structures and materials for energy absorption applications. Compos. Part B Eng. **181**, 107496 (2020). https://doi.org/10.1016/j.compositesb.2019.107496
7. P. Trogadas, M.O. Coppens, Nature-inspired electrocatalysts and devices for energy conversion. Chem. Soc. Rev. **49**(10), 3107–3141 (2020). https://doi.org/10.1039/C8CS00797G
8. N.K. Katiyar, G. Goel, S. Hawi, S. Goel, Nature-inspired materials: emerging trends and prospects. NPG Asia Mater. **13**, 56 (2021). https://doi.org/10.1038/s41427-021-00322-y
9. D. Gust, T.A. Moore, A.L. Moore, Solar fuels via artificial photosynthesis. Acc. Chem. Res. **42**(12), 1890–1898 (2009). https://doi.org/10.1021/ar900209b
10. J. Wang, T. Zhu, G.W. Ho, Nature-inspired design of artificial solar-to-fuel conversion systems based on copper phosphate microflowers. Chemsuschem **9**(13), 1575–1578 (2016). https://doi.org/10.1002/cssc.201600481
11. E. Freeman, R. Soncini, L. Weiland, Biologically inspired water purification through selective transport. Smart Mater. Struct. **22**(1), 014013 (2012). https://doi.org/10.1088/0964-1726/22/1/014013
12. N. Kronqvist, M. Sarr, A. Lindqvist, K. Nordling, M. Otikovs et al., Efficient protein production inspired by how spiders make silk. Nat. Commun. **8**, 15504 (2017). https://doi.org/10.1038/ncomms15504
13. Q.F. Guan, H.B. Yang, Z.M. Han, Z.C. Ling, S.H. Yu, An all-natural bioinspired structural material for plastic replacement. Nat. Commun. **11**, 5401 (2020). https://doi.org/10.1038/s41467-020-19174-1
14. H. Wang, Y. Yang, L. Guo, Nature-inspired electrochemical energy-storage materials and devices. Adv. Energy Mater. **7**(5), 1601709 (2017). https://doi.org/10.1002/aenm.201601709
15. W.E. Tenhaeff, O. Rios, K. More, M.A. McGuire, Highly robust lithium ion battery anodes from lignin: an abundant, renewable, and low-cost material. Adv. Funct. Mater. **24**(1), 86–94 (2014). https://doi.org/10.1002/adfm.201301420
16. S.K. Kim, Y.K. Kim, H. Lee, S.B. Lee, H.S. Park, Superior pseudocapacitive behavior of confined lignin nanocrystals for renewable energy-storage materials. Chemsuschem **7**(4), 1094–1101 (2014). https://doi.org/10.1002/cssc.201301061
17. J. Zhou, C. Zheng, H. Wang, J. Yang, P. Hu et al., 3D nest-shaped Sb_2O_3/RGO composite based high-performance lithium-ion batteries. Nanoscale **8**(39), 17131–17135 (2016). https://doi.org/10.1039/C6NR06454J
18. S. Sahoo, R. Kumar, E. Joanni, R.K. Singh, J.J. Shim, Advances in pseudocapacitive and battery-like electrode materials for high performance supercapacitors. J. Mater. Chem. A **10**(25), 13190–13240 (2022). https://doi.org/10.1039/D2TA02357A
19. I. Hussain, S. Iqbal, C. Lamiel, A. Alfantazi, K. Zhang, Recent advances in oriented metal-organic frameworks for supercapacitive energy storage. J. Mater. Chem. A **10**(9), 4475–4488 (2022). https://doi.org/10.1039/D1TA10213C
20. R. Kumar, E. Joanni, S. Sahoo, J.J. Shim, T.W. Kian et al., An overview of recent progress in nanostructured carbon-based supercapacitor electrodes: from zero to bi-dimensional materials. Carbon **193**, 298–338 (2022). https://doi.org/10.1016/j.carbon.2022.03.023
21. I. Hussain, S. Sahoo, D. Mohapatra, M. Ahmad, S. Iqbal et al., Recent progress in trimetallic/ternary-metal oxides nanostructures: misinterpretation/misconception of electrochemical data and devices. Appl. Mater. Today **26**, 101297 (2022). https://doi.org/10.1016/j.apmt.2021.101297
22. I. Hussain, S. Sahoo, C. Lamiel, T.T. Nguyen, M. Ahmed et al., Research progress and future aspects: metal selenides as effective electrodes. Energy Storage Mater. **47**, 13–43 (2022). https://doi.org/10.1016/j.ensm.2022.01.055
23. J. Yan, T. Liu, X. Liu, Y. Yan, Y. Huang, Metal-organic framework-based materials for flexible supercapacitor application. Coord. Chem. Rev. **452**, 214300 (2022). https://doi.org/10.1016/j.ccr.2021.214300
24. J. Jin, X. Geng, Q. Chen, T.L. Ren, A better Zn-ion storage device: recent progress for Zn-ion hybrid supercapacitors. Nano-Micro Lett. **14**, 64 (2022). https://doi.org/10.1007/s40820-022-00793-w
25. T. Kar, S. Godavarthi, S.K. Pasha, K. Deshmukh, L. Martínez-Gómez et al., Layered materials and their heterojunctions for supercapacitor applications: a review. Crit. Rev. Solid State Mater. Sci. **47**(3), 357–388 (2022). https://doi.org/10.1080/10408436.2021.1886048
26. H. He, J. Lian, C. Chen, Q. Xiong, C.C. Li et al., Enabling multi-chemisorption sites on carbon nanofibers cathodes by an in-situ exfoliation strategy for high-performance Zn-ion hybrid capacitors. Nano-Micro Lett. **14**, 106 (2022). https://doi.org/10.1007/s40820-022-00839-z
27. T. Xu, D. Wang, Z. Li, Z. Chen, J. Zhang et al., Electrochemical proton storage: from fundamental understanding

to materials to devices. Nano-Micro Lett. **14**, 126 (2022). https://doi.org/10.1007/s40820-022-00864-y

28. M.S. Javed, T. Najim, I. Hussain, S. Batool, M. Idrees et al., 2D V_2O_5 nanoflakes as a binder-free electrode material for high-performance pseudocapacitor. Ceram. Int. **47**(17), 25152–25157 (2021). https://doi.org/10.1016/j.ceramint.2021.05.181
29. I. Hussain, A. Ali, C. Lamiel, S.G. Mohamed, S. Sahoo et al., A 3D walking palm-like core-shell $CoMoO_4$@$NiCo_2S_4$@nickel foam composite for high-performance supercapacitors. Dalton Transact. **48**(12), 3853–3861 (2019). https://doi.org/10.1039/C8DT04045A
30. I. Hussain, T. Hussain, S.B. Ahmed, T. Kaewmaraya, M. Ahmad et al., Binder-free trimetallic phosphate nanosheets as an electrode: theoretical and experimental investigation. J. Power Sources **513**, 230556 (2021). https://doi.org/10.1016/j.jpowsour.2021.230556
31. L. Zhang, X. Hu, Z. Wang, F. Sun, D.G. Dorrell, a review of supercapacitor modeling, estimation, and applications: a control/management perspective. Renew. Sustain. Energy Rev. **81**, 1868–1878 (2018). https://doi.org/10.1016/j.rser.2017.05.283
32. S. Kumar, G. Saeed, L. Zhu, K.N. Hui, N.H. Kim et al., 0D to 3D carbon-based networks combined with pseudocapacitive electrode material for high energy density supercapacitor: a review. Chem. Eng. J. **403**, 126352 (2021). https://doi.org/10.1016/j.cej.2020.126352
33. Z. Yang, J. Tian, Z. Yin, C. Cui, W. Qian et al., Carbon nanotube-and graphene-based nanomaterials and applications in high-voltage supercapacitor: a review. Carbon **141**, 467–480 (2019). https://doi.org/10.1016/j.carbon.2018.10.010
34. A. Mohanty, D. Jaihindh, Y.P. Fu, S.P. Senanayak, L.S. Mende et al., An extensive review on three dimension architectural metal-organic frameworks towards supercapacitor application. J. Power Sources **488**, 229444 (2021). https://doi.org/10.1016/j.jpowsour.2020.229444
35. Z. Bi, Q. Kong, Y. Cao, G. Sun, F. Su et al., Biomass-derived porous carbon materials with different dimensions for supercapacitor electrodes: a review. J. Mater. Chem. A **7**(27), 16028–16045 (2019). https://doi.org/10.1039/C9TA04436A
36. D.G. Wang, Z. Liang, S. Gao, C. Qu, R. Zou, Metal-organic framework-based materials for hybrid supercapacitor application. Coord. Chem. Rev. **404**, 213093 (2020). https://doi.org/10.1016/j.ccr.2019.213093
37. A. Gopalakrishnan, S. Badhulika, Effect of self-doped heteroatoms on the performance of biomass-derived carbon for supercapacitor applications. J. Power Sources **480**, 228830 (2020). https://doi.org/10.1016/j.jpowsour.2020.228830
38. M. Ahmad, I. Hussain, T. Nawaz, Y. Li, X. Chen et al., Comparative study of ternary metal chalcogenides (MX; M= Zn-Co-Ni; X= S, Se, Te): formation process, charge storage mechanism and hybrid supercapacitor. J. Power Sources **534**, 231414 (2022). https://doi.org/10.1016/j.jpowsour.2022.231414
39. I. Hussain, T. Hussain, C. Lamiel, K. Zhang, Turning indium oxide into high-performing electrode materials via cation substitution strategy: preserving single crystalline cubic structure of 2D nanoflakes towards energy storage devices. J. Power Sources **480**, 228873 (2020). https://doi.org/10.1016/j.jpowsour.2020.228873
40. S. Gu, R. Hao, J. Chen, K. Liu, X. Chen et al., Star-shaped polyimide covalent organic framework for high-voltage lithium-ion batteries. Mater. Chem. Front. **6**(17), 2545–2550 (2022). https://doi.org/10.1039/D2QM00578F
41. S. Iqbal, A.H. Mady, Y.I. Kim, U. Javed, P.M. Shafi et al., Self-templated hollow nanospheres of B-site engineered non-stoichiometric perovskite for supercapacitive energy storage via anion-intercalation mechanism. J. Colloid Interface Sci. **600**, 729–739 (2021). https://doi.org/10.1016/j.jcis.2021.03.147
42. S. Gu, Y. Chen, R. Hao, J. Zhou, I. Hussain et al., Redox of naphthalenediimide radicals in a 3D polyimide for stable Li-ion batteries. Chem. Commun. **57**(63), 7810–7813 (2021). https://doi.org/10.1039/D1CC02426D
43. I. Hussain, T. Mak, K. Zhang, Boron-doped trimetallic Cu-Ni-Co oxide nanoneedles for supercapacitor application. ACS Appl. Nano Mater. **4**(1), 129–141 (2021). https://doi.org/10.1021/acsanm.0c02411
44. I. Hussain, C. Lamiel, S.G. Mohamed, S. Vijayakumar, A. Ali et al., Controlled synthesis and growth mechanism of zinc cobalt sulfide rods on Ni-foam for high-performance supercapacitors. J. Indust. Eng. Chem. **71**, 250–259 (2019). https://doi.org/10.1016/j.jiec.2018.11.033
45. Y. Chen, S. Gu, S. Wu, X. Ma, I. Hussain et al., Copper activated near-full two-electron Mn^{4+}/Mn^{2+} redox for mild aqueous Zn/MnO_2 battery. Chem. Eng. J. **450**, 137923 (2022). https://doi.org/10.1016/j.cej.2022.137923
46. G. Dhakal, D. Mohapatra, T.L. Tamang, M. Lee, Y.R. Lee et al., Redox-additive electrolyte-driven enhancement of the electrochemical energy storage performance of asymmetric Co_3O_4//carbon nano-onions supercapacitors. Energy **218**, 119436 (2021). https://doi.org/10.1016/j.energy.2020.119436
47. U. Zubair, D. Versaci, M. Umer, J. Amici, C. Francia et al., Lithium polysulfides immobilization exploiting formate-ion doped polyaniline wrapped carbon for long cycle life sulfur cathodes via conventional electrode processing. Mater. Today Commun. **26**, 101970 (2021). https://doi.org/10.1016/j.mtcomm.2020.101970
48. S. Kumar, I.A. Mir, Z. Ahmad, K.S. Hui, D.A. Dinh et al., Microflowers of Sn-Co-S derived from ultra-thin nanosheets for supercapacitor applications. J. Energy Storage **49**, 104084 (2022). https://doi.org/10.1016/j.est.2022.104084
49. W. Kim, H.J. Lee, S.J. Yoo, C.K. Trinh, Z. Ahmad et al., Preparation of a polymer nanocomposite via the polymerization of pyrrole: biphenyldisulfonic acid: pyrrole as a two-monomer-connected precursor on MoS_2 for electrochemical energy storage. Nanoscale **13**(11), 5868–5874 (2021). https://doi.org/10.1039/D0NR08941A
50. M.S. Javed, T. Najam, M. Sajjad, S.S.A. Shah, I. Hussain et al., Design and fabrication of highly porous 2D bimetallic sulfide ZnS/FeS composite nanosheets as an advanced

 https://doi.org/10.1007/s40820-022-00944-z

negative electrode material for supercapacitors. Energy Fuels **35**(18), 15185–15191 (2021). https://doi.org/10.1021/acs.energyfuels.1c02444

51. I. Hussain, C. Lamiel, N. Qin, S. Gu, Y. Li et al., Development of vertically aligned trimetallic Mg-Ni-Co oxide grass-like nanostructure for high-performance energy storage applications. J. Colloid Interface Sci. **582**, 782–792 (2021). https://doi.org/10.1016/j.jcis.2020.08.064
52. I. Hussain, T. Hussain, S. Yang, Y. Chen, J. Zhou et al., Integration of CuO nanosheets to Zn-Ni-Co oxide nanowire arrays for energy storage applications. Chem. Eng. J. **413**, 127570 (2020). https://doi.org/10.1016/j.cej.2020.127570
53. M.Z. Ansari, K.M. Seo, S.H. Kim, S.A. Ansari, Critical aspects of various techniques for synthesizing metal oxides and fabricating their composite-based supercapacitor electrodes: a review. Nanomaterials **12**(11), 1873 (2022). https://doi.org/10.3390/nano12111873
54. N. Abbas, I. Shaheen, I. Ali, M. Ahmad, S.A. Khan et al., Effect of growth duration of $Zn_{0.76}Co_{0.24}S$ interconnected nanosheets for high-performance flexible energy storage electrode materials. Ceram. Int. (2022). https://doi.org/10.1016/j.ceramint.2022.07.225
55. M.Z. Ansari, D.K. Nandi, P. Janicek, S.A. Ansari, R. Ramesh et al., Low-temperature atomic layer deposition of highly conformal tin nitride thin films for energy storage devices. ACS Appl. Mater. Interfaces **11**(46), 43608–43621 (2019). https://doi.org/10.1021/acsami.9b15790
56. I. Hussain, D. Mohapatra, C. Lamiel, M. Ahmad, M.A. Ashraf et al., Phosphorus containing layered quadruple hydroxide electrode materials on lab waste recycled flexible current collector. J. Colloid Interface Sci. **609**, 566–574 (2021). https://doi.org/10.1016/j.jcis.2021.11.063
57. S.G. Mohamed, I. Hussain, J.J. Shim, One-step synthesis of hollow C-$NiCo_2S_4$ nanostructures for high-performance supercapacitor electrodes. Nanoscale **10**(14), 6620–6628 (2018). https://doi.org/10.1039/C7NR07338K
58. M.S. Javed, M. Imran, M.A. Assiri, I. Hussain, S. Hussain et al., One-step synthesis of carbon incorporated 3D MnO_2 nanorods as a highly efficient electrode material for pseudocapacitors. Mater. Lett. **295**, 129838 (2021). https://doi.org/10.1016/j.matlet.2021.129838
59. S.G. Mohamed, I. Hussain, M.S. Sayed, J.J. Shim, One-step development of octahedron-like $CuCo_2O_4$@ carbon fibers for high-performance supercapacitors electrodes. J. Alloys Compd. **842**, 155639 (2020). https://doi.org/10.1016/j.jallcom.2020.155639
60. Z. Li, X. Yu, A. Gu, H. Tang, L. Wang et al., Anion exchange strategy to synthesis of porous NiS hexagonal nanoplates for supercapacitors. Nanotechnology **28**(6), 065406 (2017). https://doi.org/10.1088/1361-6528/28/6/065406
61. N. Soudi, S. Nanayakkara, N.M. Jahed, S. Naahidi, Rise of nature-inspired solar photovoltaic energy convertors. Sol. Energy **208**, 31–45 (2020). https://doi.org/10.1016/j.solener.2020.07.048
62. M.S. Javed, T. Najam, I. Hussain, S.S.A. Shah, S. Ibraheem et al., Novel 2D vanadium oxysulfide nano-spindles decorated carbon textile composite as an advanced electrode for high-performance pseudocapacitors. Mater. Lett. **303**, 130478 (2021). https://doi.org/10.1016/j.matlet.2021.130478
63. C. Lamiel, I. Hussain, O.R. Ogunsakin, K. Zhang, MXene in core-shell structures: research progress and future aspects. J. Mater. Chem. A **10**(27), 14247–14272 (2022). https://doi.org/10.1039/D2TA02255A
64. I. Hussain, T. Hussain, M. Ahmad, X. Ma, M.S. Javed et al., Modified KBBF-like material for energy storage applications: $ZnNiBo_3(OH)$ with enhanced cycle life. ACS Appl. Mater. Interfaces **14**(6), 8025–8035 (2022). https://doi.org/10.1021/acsami.1c23583
65. I. Hussain, T. Hussain, S. Yang, Y. Chen, J. Zhou et al., Integration of CuO nanosheets to Zn-Ni-Co oxide nanowires for energy storage applications. Chem. Eng. J. **413**, 127570 (2020). https://doi.org/10.1016/j.cej.2020.127570
66. R. Schneider, M.H. Facure, P.A. Chagas, R.S. Andre, D.M. Santos et al., Tailoring the surface properties of micro/nanofibers using 0D, 1D, 2D, and 3D nanostructures: a review on post-modification methods. Adv. Mater. Interfaces **8**(13), 2100430 (2021). https://doi.org/10.1002/admi.202100430
67. J.N. Tiwari, R.N. Tiwari, K.S. Kim, Zero-dimensional, one-dimensional, two-dimensional and three-dimensional nanostructured materials for advanced electrochemical energy devices. Prog. Mater. Sci. **57**(4), 724–803 (2012). https://doi.org/10.1016/j.pmatsci.2011.08.003
68. N. Abbas, I. Shaheen, I. Hussain, C. Lamiel, M. Ahmad et al., Glycerol-mediated synthesis of copper-doped zinc sulfide with ultrathin nanoflakes for flexible energy electrode materials. J. Alloys Compd. **919**, 165701 (2022). https://doi.org/10.1016/j.jallcom.2022.165701
69. U. Amara, K. Mahmood, M. Hassan, M. Hanif, M. Khalid et al., Functionalized thiazolidone-decorated lanthanum-doped copper oxide: novel heterocyclic sea sponge morphology for the efficient detection of dopamine. RSC Adv. **12**(23), 14439–14449 (2022). https://doi.org/10.1039/D2RA01406H
70. M. Sabar, U. Amara, S. Riaz, A. Hayat, M. Nasir et al., Fabrication of MoS_2 enwrapped carbon cloth as electrochemical probe for non-enzymatic detection of dopamine. Mater. Lett. **308**, 131233 (2022). https://doi.org/10.1016/j.matlet.2021.131233
71. U. Amara, B. Sarfraz, K. Mahmood, M.T. Mehran, N. Muhammad et al., Fabrication of ionic liquid stabilized MXene interface for electrochemical dopamine detection. Microchim. Acta **189**(2), 64 (2022). https://doi.org/10.1007/s00604-022-05162-3
72. U. Amara, S. Riaz, K. Mahmood, N. Akhtar, M. Nasir et al., Copper oxide integrated perylene diimide self-assembled graphitic pencil for robust non-enzymatic dopamine detection. RSC Adv. **11**(40), 25084–25095 (2021). https://doi.org/10.1039/D1RA03908C
73. I. Hussain, S. Iqbal, T. Hussain, W.L. Cheung, S.A. Khan et al., Zn-Co-MOF on solution-free CuO nanowires for flexible hybrid energy storage devices. Mater. Today Phys.

23, 100655 (2022). https://doi.org/10.1016/j.mtphys.2022.100655

74. I. Hussain, D. Mohapatra, G. Dhakal, C. Lamiel, M.S. Sayed et al., Uniform growth of ZnS nanoflakes for high-performance supercapacitor applications. J. Energy Storage **36**, 102408 (2021). https://doi.org/10.1016/j.est.2021.102408
75. I. Hussain, S.G. Mohamed, A. Ali, N. Abbas, S.M. Ammar et al., Uniform growth of Zn-Mn-Co ternary oxide nanoneedles for high-performance energy-storage applications. J. Electroanal. Chem. **837**, 39–47 (2019). https://doi.org/10.1016/j.jelechem.2019.01.052
76. W. Tian, Q. Gao, Y. Tan, K. Yang, L. Zhu et al., Bio-inspired beehive-like hierarchical nanoporous carbon derived from bamboo-based industrial by-product as a high performance supercapacitor electrode material. J. Mater. Chem. A **3**(10), 5656–5664 (2015). https://doi.org/10.1039/C4TA06620K
77. D. Puthusseri, V. Aravindan, S. Madhavi, S. Ogale, 3D microporous conducting carbon beehive by single step polymer carbonization for high performance supercapacitors: the magic of in situ porogen formation. Energy Environ. Sci. **7**(2), 728–735 (2014). https://doi.org/10.1039/C3EE42551G
78. J. Cao, J. Luo, P. Wang, X. Wang, W. Weng, Biomass-based porous carbon beehive prepared in molten KOH for capacitors. Mater. Technol. **35**(9–10), 522–528 (2020). https://doi.org/10.1080/10667857.2019.1699270
79. L. Chang, Y.H. Hu, One-step synthesis of high surface-area honeycomb graphene clusters for highly efficient capacitive deionization. J. Phys. Chem. Solids **134**, 64–68 (2019). https://doi.org/10.1016/j.jpcs.2019.05.040
80. X. Feng, Y. Huang, C. Li, Y. Xiao, X. Chen et al., Construction of carnations-like Mn_3O_4@$NiCo_2O_4$@NiO hierarchical nanostructures for high-performance supercapacitors. Electrochim. Acta **308**, 142–149 (2019). https://doi.org/10.1016/j.electacta.2019.04.048
81. X. He, P. Liu, J. Liu, Y. Muhammad, M. Zhu et al., Facile synthesis of hierarchical N-doped hollow porous carbon whiskers with ultrahigh surface area via synergistic inner-outer activation for casein hydrolysate adsorption. J. Mater. Chem. B **5**(46), 9211–9218 (2017). https://doi.org/10.1039/C7TB02345F
82. A. Gopalakrishnan, T.D. Raju, S. Badhulika, Green synthesis of nitrogen, sulfur-co-doped worm-like hierarchical porous carbon derived from ginger for outstanding supercapacitor performance. Carbon **168**, 209–219 (2020). https://doi.org/10.1016/j.carbon.2020.07.017
83. Y. Wang, X. Tang, M. Han, Y. Li, Y. Zhang et al., One-step synthesis of the N and P co-doped nest-like mesoporous carbon by a microwave-assisted ultra-high temperature solvothermal method for supercapacitor application. ChemistrySelect **4**(3), 1108–1116 (2019). https://doi.org/10.1002/slct.201803006
84. S.H. Park, S.B. Yoon, H.K. Kim, J.T. Han, H.W. Park et al., Spine-like nanostructured carbon interconnected by graphene for high-performance supercapacitors. Sci. Rep. **4**, 6118 (2014). https://doi.org/10.1038/srep06118
85. J. Liu, H. Li, H. Zhang, Q. Liu, R. Li et al., Three-dimensional hierarchical and interconnected honeycomb-like porous carbon derived from pomelo peel for high performance supercapacitors. J. Solid State Chem. **257**, 64–71 (2018). https://doi.org/10.1016/j.jssc.2017.07.033
86. Q. Liang, L. Ye, Z.H. Huang, Q. Xu, Y. Bai et al., A honeycomb-like porous carbon derived from pomelo peel for use in high-performance supercapacitors. Nanoscale **6**(22), 13831–13837 (2014). https://doi.org/10.1039/C4NR04541F
87. H. Fan, W. Liu, W. Shen, Honeycomb-like composite structure for advanced solid state asymmetric supercapacitors. Chem. Eng. J. **326**, 518–527 (2017). https://doi.org/10.1016/j.cej.2017.05.121
88. T. Liu, Y. Zheng, W. Zhao, L. Cui, J. Liu, Uniform generation of $NiCo_2S_4$ with 3D honeycomb-like network structure on carbon cloth as advanced electrode materials for flexible supercapacitors. J. Colloid Interface Sci. **556**, 743–752 (2019). https://doi.org/10.1016/j.jcis.2019.08.094
89. C.M. Chen, Q. Zhang, X.C. Zhao, B. Zhang, Q.Q. Kong et al., Hierarchically aminated graphene honeycombs for electrochemical capacitive energy storage. J. Mater. Chem. **22**(28), 14076–14084 (2012). https://doi.org/10.1039/c2jm31426f
90. P.X. Thinh, C. Basavaraja, D. Kim, Characterization and electrochemical behaviors of honeycomb-patterned poly (N-vinylcarbazole)/polystyrene composite films. Polym. Bull. **69**(1), 81–94 (2012). https://doi.org/10.1007/s00289-012-0727-9
91. L.G. Beka, X. Li, X. Wang, C. Han, W. Liu, A hierarchical $NiCo_2S_4$ honeycomb/$NiCo_2S_4$ nanosheet core-shell structure for supercapacitor applications. RSC Adv. **9**(55), 32338–32347 (2019). https://doi.org/10.1039/C9RA05840K
92. H.W. Nam, C.V.V.M. Gopi, S. Sambasivam, R. Vinodh, K.V.G. Raghavendra et al., Binder-free honeycomb-like $FeMoO_4$ nanosheet arrays with dual properties of both battery-type and pseudocapacitive-type performances for supercapacitor applications. J. Energy Storage **27**, 101055 (2020). https://doi.org/10.1016/j.est.2019.101055
93. E. Samuel, A. Aldalbahi, M. El-Newehy, H. El-Hamshary, S.S. Yoon, Nickel ferrite beehive-like nanosheets for binder-free and high-energy-storage supercapacitor electrodes. J. Alloys Compd. **852**, 156929 (2021). https://doi.org/10.1016/j.jallcom.2020.156929
94. L. Yao, G. Yang, P. Han, Z. Tang, J. Yang, Three-dimensional beehive-like hierarchical porous polyacrylonitrile-based carbons as a high performance supercapacitor electrodes. J. Power Sources **315**, 209–217 (2016). https://doi.org/10.1016/j.jpowsour.2016.03.006
95. M. Ding, G. Chen, W. Xu, C. Jia, H. Luo, Bio-inspired synthesis of nanomaterials and smart structures for electrochemical energy storage and conversion. Nano Mater. Sci. **2**(3), 264–280 (2020). https://doi.org/10.1016/j.nanoms.2019.09.011
96. A. Zhang, H. Bai, L. Li, Breath figure: a nature-inspired preparation method for ordered porous films. Chem. Rev. **115**(18), 9801–9868 (2015). https://doi.org/10.1021/acs.chemrev.5b00069

 https://doi.org/10.1007/s40820-022-00944-z

97. Q. Zhang, X. Yang, P. Li, G. Huang, S. Feng et al., Bioinspired engineering of honeycomb structure-using nature to inspire human innovation. Prog. Mater. Sci. **74**, 332–400 (2015). https://doi.org/10.1016/j.pmatsci.2015.05.001
98. D.R. Kumar, K.R. Prakasha, A.S. Prakash, J.J. Shim, Direct growth of honeycomb-like $NiCo_2O_4$@Ni foam electrode for pouch-type high-performance asymmetric supercapacitor. J. Alloys Compd. **836**, 155370 (2020). https://doi.org/10.1016/j.jallcom.2020.155370
99. X. Wu, L. Jiang, C. Long, Z. Fan, From flour to honeycomb-like carbon foam: carbon makes room for high energy density supercapacitors. Nano Energy **13**, 527–536 (2015). https://doi.org/10.1016/j.nanoen.2015.03.013
100. Z. Lv, Y. Tang, Z. Zhu, J. Wei, W. Li et al., Honeycomb-lantern-inspired 3D stretchable supercapacitors with enhanced specific areal capacitance. Adv. Mater. **30**(50), 1805468 (2018). https://doi.org/10.1002/adma.201805468
101. S. Sun, J. Luo, Y. Qian, Y. Jin, Y. Liu et al., Metal-organic framework derived honeycomb Co_9S_8@C composites for high-performance supercapacitors. Adv. Energy Mater. **8**(25), 1801080 (2018). https://doi.org/10.1002/aenm.201801080
102. Z. Peng, X. Liu, H. Meng, Z. Li, B. Li et al., Design and tailoring of the 3D macroporous hydrous RuO_2 hierarchical architectures with a hard-template method for high-performance supercapacitors. ACS Appl. Mater. Interfaces **9**(5), 4577–4586 (2017). https://doi.org/10.1021/acsami.6b12532
103. E. Raymundo-Piñero, M. Cadek, F. Béguin, Tuning carbon materials for supercapacitors by direct pyrolysis of seaweeds. Adv. Funct. Mater. **19**(7), 1032–1039 (2009). https://doi.org/10.1002/adfm.200801057
104. Q. Wang, J. Yan, T. Wei, J. Feng, Y. Ren et al., Two-dimensional mesoporous carbon sheet-like framework material for high-rate supercapacitors. Carbon **60**, 481–487 (2013). https://doi.org/10.1016/j.carbon.2013.04.067
105. T. Sun, L. Feng, X. Gao, L. Jiang, Bioinspired surfaces with special wettability. Acc. Chem. Res. **38**(8), 644–652 (2005). https://doi.org/10.1021/ar040224c
106. L. Jiang, Y. Zhao, J. Zhai, A lotus-leaf-like superhydrophobic surface: a porous microsphere/nanofiber composite film prepared by electrohydrodynamics. Angwn. Chem. Int. Ed. **43**(33), 4338–4341 (2004). https://doi.org/10.1002/anie.200460333
107. Y. Zheng, H. Bai, Z. Huang, X. Tian, F.Q. Nie et al., Directional water collection on wetted spider silk. Nature **463**(7281), 640–643 (2010). https://doi.org/10.1038/nature08729
108. J. Sun, R.N. Zuckermann, Peptoid polymers: a highly designable bioinspired material. ACS Nano **7**(6), 4715–4732 (2013). https://doi.org/10.1021/nn4015714
109. M.E. McConney, K.D. Anderson, L.L. Brott, R.R. Naik, V.V. Tsukruk, Bioinspired material approaches to sensing. Adv. Funct. Mater. **19**(16), 2527–2544 (2009). https://doi.org/10.1002/adfm.200900606
110. X. Deng, S. Zhu, J. Li, F. He, E. Liu et al., Bio-inspired three-dimensional carbon network with enhanced mass-transfer ability for supercapacitors. Carbon **143**, 728–735 (2018). https://doi.org/10.1016/j.carbon.2018.11.055
111. X. Deng, S. Zhu, J. Li, F. He, E. Liu et al., Bio-inspired three-dimensional carbon network with enhanced mass-transfer ability for supercapacitors. Carbon **143**, 728–735 (2019). https://doi.org/10.1016/j.carbon.2018.11.055
112. S. Boukhalfa, K. Evanoff, G. Yushin, Atomic layer deposition of vanadium oxide on carbon nanotubes for high-power supercapacitor electrodes. Energy Environ. Sci. **5**(5), 6872–6879 (2012). https://doi.org/10.1039/c2ee21110f
113. M.A. Elsaid, A.Z. Sayed, A.M. Ashmawy, A.A. Hassan, A.F. Waheed et al., Hierarchically nanocoral reefs-like $ZnCo_2S_4$ deposited on Ni foam as an electrode material for high-performance battery-type symmetric supercapacitor. Bull. Tabbin Inst. Metall. Stud. (2022). https://doi.org/10.21608/tims.2022.147815.1003
114. M.S. Javed, A. Mateen, S. Ali, X. Zhang, I. Hussain et al., The emergence of 2D MXenes based Zn-ion batteries: recent development and prospects. Small **18**(26), 2201989 (2022). https://doi.org/10.1002/smll.202201989
115. I. Hussain, D. Mohapatra, G. Dhakal, C. Lamiel, S.G. Mohamed et al., Different controlled nanostructures of Mn-doped ZnS for high-performance supercapacitor applications. J. Energy Storage **32**, 101767 (2020). https://doi.org/10.1016/j.est.2020.101767
116. I. Hussain, C. Lamiel, N. Qin, S. Gu, Y. Li et al., Development of vertically aligned trimetallic Mg-Ni-Co oxide grass-like nanostructure for high-performance energy storage applications. J. Colloid Interface Sci. **582**, 782–792 (2020). https://doi.org/10.1016/j.jcis.2020.08.064
117. M.S. Javed, T. Najim, I. Hussain, S. Batool, M. Idrees et al., 2D V_2O_5 nanoflakes as a binder-free electrode material for high-performance pseudocapacitor. Ceram. Int. **47**(17), 25152–25157 (2021). https://doi.org/10.1016/j.ceramint.2021.05.181
118. R. Manikandan, C.J. Raj, M. Rajesh, B.C. Kim, G. Nagaraju et al., Rationally designed spider web-like trivanadium heptaoxide nanowires on carbon cloth as a new class of pseudocapacitive electrode for symmetric supercapacitors with high energy density and ultra-long cyclic stability. J. Mater. Chem. A **6**(24), 11390–11404 (2018). https://doi.org/10.1039/C8TA03011A
119. P. Sun, W. He, H. Yang, R. Cao, J. Yin et al., Hedgehog-inspired nanostructures for hydrogel-based all-solid-state hybrid supercapacitors with excellent flexibility and electrochemical performance. Nanoscale **10**(40), 19004–19013 (2018). https://doi.org/10.1039/C8NR04919J
120. Y. Tao, L. Zaijun, L. Ruiyi, N. Qi, K. Hui et al., Nickel-cobalt double hydroxides microspheres with hollow interior and hedgehog-like exterior structures for supercapacitors. J. Mater. Chem. **22**(44), 23587–23592 (2012). https://doi.org/10.1039/c2jm35263j
121. H. Wan, J. Jiang, Y. Ruan, J. Yu, L. Zhang et al., Direct formation of hedgehog-like hollow Ni-Mn oxides and sulfides for supercapacitor electrodes. Part. Part. Syst. Charact. **31**(8), 857–862 (2014). https://doi.org/10.1002/ppsc.201400020

122. Y. Luo, J. Jiang, W. Zhou, H. Yang, J. Luo et al., Self-assembly of well-ordered whisker-like manganese oxide arrays on carbon fiber paper and its application as electrode material for supercapacitors. J. Mater. Chem. **22**(17), 8634–8640 (2012). https://doi.org/10.1039/c2jm16419a
123. J. Wei, J. Zhang, Y. Liu, G. Xu, Z. Chen et al., Controlled growth of whisker-like polyaniline on carbon nanofibers and their long cycle life for supercapacitors. RSC Adv. **3**(12), 3957–3962 (2013). https://doi.org/10.1039/c3ra23040f
124. Y. Tang, Y. Liu, W. Guo, S. Yu, F. Gao, Floss-like Ni-Co binary hydroxides assembled by whisker-like nanowires for high-performance supercapacitor. Ionics **21**(6), 1655–1663 (2015). https://doi.org/10.1007/s11581-014-1319-5
125. K. Khawas, P. Kumari, S. Daripa, R. Oraon, B.K. Kuila, Hierarchical polyaniline-MnO_2-reduced graphene oxide ternary nanostructures with whiskers-like polyaniline for supercapacitor application. ChemistrySelect **2**(35), 11783–11789 (2017). https://doi.org/10.1002/slct.201702345
126. X. Chen, D. Chen, X. Guo, R. Wang, H. Zhang, Facile growth of caterpillar-like $NiCo_2S_4$ nanocrystal arrays on nickle foam for high-performance supercapacitors. ACS Appl. Mater. Interfaces **9**(22), 18774–18781 (2017). https://doi.org/10.1021/acsami.7b03254
127. Y. Yang, Y. Hao, J. Yuan, L. Niu, F. Xia, In situ preparation of caterpillar-like polyaniline/carbon nanotube hybrids with core shell structure for high performance supercapacitors. Carbon **78**, 279–287 (2014). https://doi.org/10.1016/j.carbon.2014.07.004
128. Z. Liu, K. Xiao, H. Guo, X. Ning, A. Hu et al., Nitrogen-doped worm-like graphitized hierarchical porous carbon designed for enhancing area-normalized capacitance of electrical double layer supercapacitors. Carbon **117**, 163–173 (2017). https://doi.org/10.1016/j.carbon.2017.02.087
129. D. Yuan, J. Chen, S. Tan, N. Xia, Y. Liu, Worm-like mesoporous carbon synthesized from metal-organic coordination polymers for supercapacitors. Electrochem. Commun. **11**(6), 1191–1194 (2009). https://doi.org/10.1016/j.elecom.2009.03.045
130. X. Tian, X. Li, T. Yang, K. Wang, H. Wang et al., Porous worm-like $NiMoO_4$ coaxially decorated electrospun carbon nanofiber as binder-free electrodes for high performance supercapacitors and lithium-ion batteries. Appl. Surf. Sci. **434**, 49–56 (2018). https://doi.org/10.1016/j.apsusc.2017.09.153
131. P. Yang, Y. Li, Z. Lin, Y. Ding, S. Yue et al., Worm-like amorphous MnO_2 nanowires grown on textiles for high-performance flexible supercapacitors. J. Mater. Chem. A **2**(3), 595–599 (2014). https://doi.org/10.1039/C3TA14275B
132. N. Tantawy, F.E.T. Heakal, S. Ahmed, Synthesis of worm-like binary metallic active material by electroless deposition approach for high-performance supercapacitor. J. Energy Storage **31**, 101625 (2020). https://doi.org/10.1016/j.est.2020.101625
133. L. Jinlong, L. Tongxiang, Y. Meng, K. Suzuki, H. Miura, The plume-like Ni_3S_2 supercapacitor electrodes formed on nickel foam by catalysis of thermal reduced graphene oxide. J. Electroanal. Chem. **786**, 8–13 (2017). https://doi.org/10.1016/j.jelechem.2017.01.004
134. J.Y. Liang, C.C. Wang, S.Y. Lu, Glucose-derived nitrogen-doped hierarchical hollow nest-like carbon nanostructures from a novel template-free method as an outstanding electrode material for supercapacitors. J. Mater. Chem. A **3**(48), 24453–24462 (2015). https://doi.org/10.1039/C5TA08007J
135. D. Dubal, C. Lokhande, Significant improvement in the electrochemical performances of nano-nest like amorphous MnO_2 electrodes due to Fe doping. Ceram. Int. **39**(1), 415–423 (2013). https://doi.org/10.1016/j.ceramint.2012.06.042
136. S.F. Shaikh, F.F. Shaikh, A.V. Shaikh, M. Ubaidullah, A.M. Al-Enizi et al., Electrodeposited more-hydrophilic nano-nest polyaniline electrodes for supercapacitor application. J. Phys. Chem. Solids **149**, 109774 (2021). https://doi.org/10.1016/j.jpcs.2020.109774
137. D. Zhao, Q. Zhu, D. Chen, X. Li, Y. Yu et al., Nest-like V_3O_7 self-assembled by porous nanowires as an anode supercapacitor material and its performance optimization through bonding with n-doped Carbon. J. Mater. Chem. A **6**(34), 16475–16484 (2018). https://doi.org/10.1039/C8TA06820H
138. L. Mi, W. Wei, S. Huang, S. Cui, W. Zhang et al., A nest-like $Ni@Ni_{1.4}Co_{1.6}S_2$ electrode for flexible high-performance rolling supercapacitor device design. J. Mater. Chem. A **3**(42), 20973–20982 (2015). https://doi.org/10.1039/C5TA06265A
139. F. Ran, H. Fan, L. Wang, L. Zhao, Y. Tan et al., A bird nest-like manganese dioxide and its application as electrode in supercapacitors. J. Energy Chem. **22**(6), 928–934 (2013). https://doi.org/10.1016/S2095-4956(14)60274-6
140. Y. Huang, F. Cui, Y. Zhao, J. Lian, J. Bao et al., $NiMoO_4$ nanorod deposited carbon sponges with ant-nest-like interior channels for high-performance pseudocapacitors. Inorg. Chem. Front. **5**(7), 1594–1601 (2018). https://doi.org/10.1039/C8QI00247A
141. F. Miao, N. Lu, P. Zhang, Z. Zhang, G. Shao, Multidimension-controllable synthesis of ant nest-structural electrode materials with unique 3D hierarchical porous features toward electrochemical applications. Adv. Funct. Mater. **29**(29), 1808994 (2019). https://doi.org/10.1002/adfm.201808994
142. Q. Lu, X. Wang, M. Chen, B. Lu, M. Liu et al., Manganese dioxide/ant-nest-like hierarchical porous carbon composite with robust supercapacitive performances. ACS Sustain. Chem. Eng. **6**(6), 7362–7371 (2018). https://doi.org/10.1021/acssuschemeng.7b04492
143. F. Wang, L. Chen, H. Li, G. Duan, S. He et al., N-doped honeycomb-like porous carbon towards high-performance supercapacitor. Chin. Chem. Lett. **31**(7), 1986–1990 (2020). https://doi.org/10.1016/j.cclet.2020.02.020
144. Y. Wang, Z. Zhao, W. Song, Z. Wang, X. Wu, From biological waste to honeycomb-like porous carbon for high energy density supercapacitor. J. Mater. Sci. **54**(6), 4917–4927 (2019). https://doi.org/10.1007/s10853-018-03215-8
145. X. Ren, C. Guo, L. Xu, T. Li, L. Hou et al., Facile synthesis of hierarchical mesoporous honeycomb-like NiO for

 https://doi.org/10.1007/s40820-022-00944-z

aqueous asymmetric supercapacitors. ACS Appl. Mater. Interfaces **7**(36), 19930–19940 (2015). https://doi.org/10.1021/acsami.5b04094

146. G.K. Veerasubramani, A. Chandrasekhar, M. Sudhakaran, Y.S. Mok, S.J. Kim, Liquid electrolyte mediated flexible pouch-type hybrid supercapacitor based on binderless core-shell nanostructures assembled with honeycomb-like porous Carbon. J. Mater. Chem. A **5**(22), 11100–11113 (2017). https://doi.org/10.1039/C7TA01308F
147. J. Wang, F. Qin, Z. Guo, W. Shen, Oxygen- and nitrogen-enriched honeycomb-like porous carbon from Laminaria japonica with excellent supercapacitor performance in aqueous solution. ACS Sustain. Chem. Eng. **7**(13), 11550–11563 (2019). https://doi.org/10.1021/acssuschemeng.9b01448
148. A. Ali, M. Aadil, A. Rasheed, I. Hameed, S. Ajmal et al., Honeycomb like architectures of the Mo doped ZnS@Ni for high-performance asymmetric supercapacitors applications. Synth. Met. **265**, 116408 (2020). https://doi.org/10.1016/j.synthmet.2020.116408
149. R. Kumar, S.M. Youssry, H.M. Soe, M.M. Abdel-Galeil, G. Kawamura et al., Honeycomb-like open-edged reduced-graphene-oxide-enclosed transition metal oxides (NiO/Co_3O_4) as improved electrode materials for high-performance supercapacitor. J. Energy Storage **30**, 101539 (2020). https://doi.org/10.1016/j.est.2020.101539
150. X. Dong, Y. Yu, X. Jing, H. Jiang, T. Hu et al., Sandwich-like honeycomb Co_2SiO_4/rGO/honeycomb Co_2SiO_4 structures with enhanced electrochemical properties for high-performance hybrid supercapacitor. J. Power Sources **492**, 229643 (2021). https://doi.org/10.1016/j.jpowsour.2021.229643
151. L. Du, W. Du, H. Ren, N. Wang, Z. Yao et al., Honeycomb-like metallic nickel selenide nanosheet arrays as binder-free electrodes for high-performance hybrid asymmetric supercapacitors. J. Mater. Chem. A **5**(43), 22527–22535 (2017). https://doi.org/10.1039/C7TA06921A
152. L. Cao, S. Yang, W. Gao, Z. Liu, Y. Gong et al., Direct laser-patterned micro-supercapacitors from paintable MoS_2 films. Small **9**(17), 2905–2910 (2013). https://doi.org/10.1002/smll.201203164
153. X. Chen, S. Wang, J. Shi, X. Du, Q. Cheng et al., Direct laser etching free-standing MXene-MoS_2 film for highly flexible micro-supercapacitor. Adv. Mater. Interfaces **6**(22), 1901160 (2019). https://doi.org/10.1002/admi.201901160
154. S.K. Kim, H.J. Koo, A. Lee, P.V. Braun, Selective wetting-induced micro-electrode patterning for flexible micro-supercapacitors. Adv. Mater. **26**(30), 5108–5112 (2014). https://doi.org/10.1002/adma.201401525
155. L. Liu, D. Ye, Y. Yu, L. Liu, Y. Wu, Carbon-based flexible micro-supercapacitor fabrication via mask-free ambient micro-plasma-jet etching. Carbon **111**, 121–127 (2017). https://doi.org/10.1016/j.carbon.2016.09.037
156. W. Sun, X. Chen, Preparation and characterization of polypyrrole films for three-dimensional micro supercapacitor. J. Power Sources **193**(2), 924–929 (2009). https://doi.org/10.1016/j.jpowsour.2009.04.063
157. D. Qi, Y. Liu, Z. Liu, L. Zhang, X. Chen, Design of architectures and materials in in-plane micro-supercapacitors: current status and future challenges. Adv. Mater. **29**(5), 1602802 (2017). https://doi.org/10.1002/adma.201602802
158. S. Wang, N. Liu, J. Rao, Y. Yue, K. Gao et al., Vertical finger-like asymmetric supercapacitors for enhanced performance at high mass loading and inner integrated photodetecting systems. J. Mater. Chem. A **5**(42), 22199–22207 (2017). https://doi.org/10.1039/C7TA06306G
159. A.V. Salkar, A.P. Naik, S.V. Bhosale, P.P. Morajkar, Designing a rare DNA-like double helical microfiber superstructure via self-assembly of in situ carbon fiber-encapsulated Wo_{3-x} nanorods as an advanced supercapacitor material. ACS Appl. Mater. Interfaces **13**(1), 1288–1300 (2020). https://doi.org/10.1021/acsami.0c21105
160. P. Avasthi, V. Balakrishnan, Electroless growth of high surface area Au dendrites with corrugated edge structure for hybrid supercapacitor applications. ChemistrySelect **3**(13), 3866–3870 (2018). https://doi.org/10.1002/slct.201703132
161. H. Pang, F. Gao, Q. Chen, R. Liu, Q. Lu, Dendrite-like Co_3O_4 nanostructure and its applications in sensors, supercapacitors and catalysis. Dalton Transact. **41**(19), 5862–5868 (2012). https://doi.org/10.1039/c2dt12494g
162. Y. Zhao, M. Dai, D. Zhao, L. Xiao, X. Wu et al., Asymmetric pseudo-capacitors based on dendrite-like MnO_2 nanostructures. CrystEngComm **21**(21), 3349–3355 (2019). https://doi.org/10.1039/C9CE00423H
163. Z. Sun, S. Firdoz, E.Y.X. Yap, L. Li, X. Lu, Hierarchically structured MnO_2 nanowires supported on hollow Ni dendrites for high-performance supercapacitors. Nanoscale **5**(10), 4379–4387 (2013). https://doi.org/10.1039/c3nr00209h
164. S. Iqbal, A.H. Mady, U. Javed, P.M. Shafi, N.V. Quang et al., Self-templated hollow nanospheres of b-site engineered non-stoichiometric perovskite for supercapacitive energy storage via anion-intercalation mechanism. J. Colloid Interface Sci. **600**, 729–739 (2021). https://doi.org/10.1016/j.jcis.2021.03.147
165. I. Hussain, J.M. Lee, S. Iqbal, H.S. Kim, S.W. Jang et al., Preserved crystal phase and morphology: electrochemical influence of copper and iron co-doped cobalt oxide and its supercapacitor applications. Electrochim. Acta **340**, 135953 (2020). https://doi.org/10.1016/j.electacta.2020.135953
166. I. Hussain, C. Lamiel, M. Ahmad, Y. Chen, S. Shuang et al., High entropy alloys as electrode material for supercapacitors: a review. J. Energy Storage **44**, 103405 (2021). https://doi.org/10.1016/j.est.2021.103405
167. T.S. Mathis, N. Kurra, X. Wang, D. Pinto, P. Simon et al., Energy storage data reporting in perspective-guidelines for interpreting the performance of electrochemical energy storage systems. Adv. Energy Mater. **9**(39), 1902007 (2019). https://doi.org/10.1002/aenm.201902007